José Miguel Marques Caetano

Development of an Odor Compass: 2D Thermal Anemometer with Olfactory Information

February 2017

· U C ·

Universidade de Coimbra

FCTUC FACULDADE DE CIÊNCIAS
E TECNOLOGIA
UNIVERSIDADE DE COIMBRA

Development of an Odor Compass: 2D Thermal Anemometer with Olfactory Information

José Miguel Marques Caetano

Coimbra, February 2017

Development of an Odor Compass: 2D Thermal Anemometer with Olfactory Information

Supervisor:

Prof Dr. Lino José Forte Marques

Jury:

Prof. Dr. António Paulo Mendes Breda Dias Coimbra

Prof. Dr. Mário João Simões Ferreira dos Santos

Prof. Dr. Lino José Forte Marques

Dissertation submitted in partial fulfillment for the degree of Master of Science in Electrical and Computer Engineering.

Coimbra, February 2017

Agradecimentos

Aos meus pais José e Maria e à minha irmã Daniela, agradeço a paciência, o amor e todo o apoio incondicional dados ao longo de todos estes anos. A eles devo tudo o que sou.

À minha namorada, Ana, agradeço todo o tempo despendido, o apoio permanente e, sobretudo, a compreensão, amizade e amor, que me aqueceram nas épocas mais frias deste percurso.

Um agradecimento especial ao meu orientador, Professor Doutor Lino Marques, pela sua disponibilidade, por todo o apoio ao longo deste projeto e, acima de tudo, pela sua orientação.

Ao Laboratório de Sistemas Embebidos do Instituto de Sistemas e Robótica da Universidade de Coimbra, especialmente ao Eduardo e ao João que foram, sem dúvida, determinantes no meu trabalho, um obrigado pela hospitalidade, pelos momentos de descontração e por toda a ajuda prestada.

Por último, mas não menos importante, agradeço a todos os meus familiares e amigos por toda a força e apoio, pelos momentos de lazer e principalmente por permanecerem.

A todos, o meu sincero obrigado!

Resumo

Muitos animais usam o olfato como um sentido de orientação combinando a informação sobre a concentração de um odor específico, presente no ar, e a velocidade do vento. Este tipo de deteção está ligado aos conceitos de deteção baseados em quimiotaxia e anemotaxia, uma vez que se consideram as propriedades químicas e eólicas aquando da localização da origem de um odor. No entanto, o olfato é muitas vezes desprezado, pelos seres humanos, como um sentido de orientação, não sendo, portanto, objeto de profunda investigação e/ou desenvolvimento. Assim, esta tese pretende dar uma contribuição nesta área através do desenvolvimento de um compasso de odores baseado em métodos térmicos, para medir as propriedades de um fluido, e um sensor de gás eletroquímico, de forma a medir a concentração do odor. Os compassos de odor são adequados para o uso em robôs móveis, possibilitando o rastreamento ativo de um odor, e em redes de sensores ambientais, permitindo um rastreamento estático de odor. Estes podem, portanto, ser usados em aplicações como o controlo de ambientes de vida e de trabalho num edifício, inspeção de ambientes perigosos utilizando robôs móveis, deteção de drogas e explosivos, e deteção precoce de incêndios florestais. Para desenvolver tal dispositivo, foram colocados vários termístores, também designados de elementos aquecidos, em torno de uma estrutura triangular, permitindo que a relação entre as suas respostas possa ser utilizada para determinar a direção da origem de um odor enquanto se usa um sensor de gás de óxidos metálicos para medir a concentração do mesmo.

Testes em laboratório realizados com etanol, de forma a produzir a quantidade desejada de odor, e um processo de calibração completamente automatizado, mostraram que o sensor desenvolvido consegue indicar a direção da origem de um odor com precisão, medindo a velocidade do fluxo de ar com um erro absoluto médio de 0,0245 m/s e a direção do fluxo de ar com um erro absoluto médio de 3%.

Palavras-chave: Localização de Fontes Odoríferas, Compasso de Odor, Nariz Eletrónico, Anemometria Térmica, Medição de Fluxo em Fluidos.

Abstract

Many animals use olfaction as a sense of orientation by combining the information regarding the concentration of a specific odor present in the air and the velocity of the wind. This type of detection is linked to the concepts of chemotaxis and anemotaxis based detection, since both chemical and wind properties are considered when locating the source of an odor. However, olfaction is often disregarded by humans as a sense of orientation, thus not being subject of deep research and/or development. Therefore, this thesis intends to give a contribution in this area through the development of an odor compass based on thermal methods for measuring the flow properties of a fluid and an electrochemical gas sensor for measuring its odor concentration. Odor compasses are suitable for usage in both mobile robots, in order to perform an active odor tracing, and environmental sensor networks, allowing for a static odor tracing. They can, therefore, be used in applications like control of living and working environments in a building, inspection of dangerous environments with mobile robots, drugs and explosives detection and earlier detection of active wildfires. To develop such a device, multiple thermistors, also referred to as heated elements, were placed around a triangular structure, so that the relation between their responses can be used to determine the direction of the odor source, while a metal oxide gas sensor was used to measure the odor concentration.

Indoor experiments realized with ethanol, in order to produce the desired amount of odor, and a fully automated calibration process showed that the developed sensor could indicate the direction of the odor source with precision, measuring the airflow velocity with a mean absolute error of 0.0245 m/s and the airflow direction with a 3% mean absolute error.

Keywords: Odor Source Localization, Odor Compass, Thermal Anemometry, Electronic Nose, Fluid Flow Measurement.

"Once we accept our limits, we go beyond them."

— Albert Einstein

Contents

List of Acronyms

MOX	Metal Oxide
MOS	Metal Oxide Semiconductor
LDA	Laser Doppler Anemometer
MEMS	Micro-Electro-Mechanical Systems
ISR	Institute of Systems and Robotics
CCA	Constant Current Anemometer
CVA	Constant Voltage Anemometer
CTA	Constant Temperature Anemometer
CPA	Constant Power Anemometer
NTC	Negative Temperature Coefficient
PTC	Positive Temperature Coefficient
PCB	Printed Circuit Board
ADC	Analog-to-Digital Converter
SMD	Surface-Mount Design
PLL	Phase-Locked-Loop
EEPROM	Electrically Erasable Programmable Read-Only Memory
UART	Universal Asynchronous Receiver Transmitter
SPI	Serial Peripheral Interface
$\boldsymbol{I^2C}$	Inter-Integrated Circuit
TTL	Transistor–Transistor Logic
PWM	Pulse-Width Modulation

List of Figures

List of Tables

1 Introduction

The human being is one of the most studied animals by Science, there being a lot of simple questions which already have an answer: we have two eyes in order to have a good peripheral vision and see in depth; we have two ears so we can have stereophonic hearing; etc. But why do we have two nostrils? Some say that certain nostrils are, temporarily, better at detecting different smells; others say that there is not a specific reason and that it is a question of development.

The fact that we cannot uniformly answer a simple question like "why do we, as well as most animals, have two nostrils?" means that there is still a lot of research to be made about smell. This leads to another question, which is: "How can animals detect an odor source?" Insects, along with other animals, make use of a combination of information regarding the velocity of the wind and the concentration of a specific odor present in the air allowing them to determine the direction which leads to the odor source location and, consequently, to locate food, mates and detect danger.

This behavior gave rise to multiple studies on how insects determine the source of an odor, existing several opinions divided between pure chemotaxis and pure anemotaxis. These are two methods that usually are not completely isolated from each other when it comes to odor detection. The first, chemotaxis, consists of following a certain odor through the increase in concentration of a certain substance in the surrounding air, while anemotaxis is based on following the direction of the airflow where the substance is detected. To transport this into the world of sensors, one needs to integrate multiple sensors into a single device, in order to measure air flow characteristics and detect a certain substance. Specifically, to be able to conjugate chemotaxis and anemotaxis, the device has to not just detect but measure the concentration of the substance in question as well as measure velocity and detect direction of the airflow. Such a device is often called odor compass.

A device with the above features could be used as, either a part of a mobile robot (active odor tracing), or in a sensor network (static odor tracing), or even a combination of both.

With that said, it would be a promising tool in various fields and applications, such as:

- Control of living and working environments in a building;
- Inspection of dangerous environments with mobile robots;
- Drugs and explosives detection;
- Earlier detection of active wildfires.

In consideration of the foregoing, this work intends to develop a sensor that integrates both chemotaxis and anemotaxis based detection, while being able to be used in mobile and static environments.

1.1 Motivation

In the last decades there has been a growing interest regarding the localization of odoriferous sources through electronic means. Part of the developments made in this area were achieved by mimicking the animal behavior through systems that can take advantage of olfaction. However, this is still an area in which much remains to be researched and developed. One of the main motivations for this thesis is the fact that odor compasses, integrating both chemotaxis and anemotaxis based detection, have not been subject of deep research and/or development. This can be explained by the reduced importance given to odor when it comes to orientation. Another important reason which serves as motivation for this thesis is the production of a single device which can be used in the fields and applications mentioned above.

1.2 Objectives

As previously referred, an odor compass is a device capable of detecting the presence of certain substances in the atmosphere and measure the direction and intensity of the wind in order to estimate the origin of the detected substances. In order to do so, a device composed of a gas sensor and a directional anemometer will be developed.

It is intended to design a robust device with reduced dimensions suitable for usage in both mobile robots and environmental sensor networks composed by nodes where it is essential to ensure low-power consumption. One main objective throughout this project is also to develop a simple yet effective sensor, ensuring a low price of production, fulfilling one of the main requirements of sensor networks.

With that said, the implementation of this work can be divided into three main parts: prototype of a mechanical structure with certain aerodynamic characteristics that allows for the detection of the wind's direction and the presence of certain odors; development of electronics ensuring a low-power consumption; and micro-controller programming to obtain a standalone smart sensor.

The first step requires simulations in terms of geometric forms and aerodynamics. In these simulations is also important to consider the electronics that will be in contact with the air flow, so that turbulence can be studied in terms of the sizes used, and how it will impact readings. In terms of electronics, it is also important to consider what is expected from the sensor regarding dynamic responses. It is also known that every sensor, when working with analog signals needs some calibration. Allying electronics and the usage of a micro-controller unit, with some active components, this calibration can be an automated process with little to no user interaction. This is also a goal for this project.

1.3 Document Overview

In terms of written content, this thesis is also divided into three parts. The first part presents an overview on odor compasses and methods regarding odor detection, while the second part describes the theoretical fundamentals which support the odor detection. Regarding the third and last part, it describes the development of an odor compass. Below is a brief description of each chapter.

Chapter 2, Odor Detection, represents the principle of detection of the most used sensors regarding artificial olfaction and describes the most common methods to measure the velocity of a fluid, focusing on thermal anemometry, which is essential to better understand the rest of this thesis. This chapter also gives a context on what has been done in terms of odor compasses.

Chapter 3, Materials and Methods, gives an explanation of some theoretical fundamentals behind the fluid flow measurement and metal oxide gas sensors as a support to the proposed solution.

Chapter 4, Odor Compass, describes the developed odor compass through the analysis of the sensor's structure, the electronics involved and the processing required.

Ultimately, chapter 5, Tests and Characterization, describes the calibration environment used to execute a set of tests as well as the results obtained from the tests' execution. These results will then be used to calibrate and validate the developed sensor.

2 Odor Detection

2.1 Defining the Odor

The odor results from the volatilization of chemical compounds, generally at a very low concentration, that humans or other animals perceive by the sense of olfaction. Olfaction is the oldest sense as per the evolutionary point of view, allowing for seeking food, recognizing danger or communication. Human olfaction can also be defined as a protective sense, since it allows the detection of potential pathologies or contamination by taking into consideration the odor pleasantness or unpleasantness [1].

The human olfactory system, for instance, has multiple cells, but the ones responsible for the odor perception are the olfactory cells. The cells' cilia are responsible for the chemical reception and further transmission of the gathered information to the olfactory nerve. Thus, the stimuli are carried from the nose to the central nervous system, where the information can be understood as an odor [2]. Therefore, the human being can recognize a large variety (in the order of thousands) of odors, using millions of olfactory receptors of about 1000 different classes. In a similar way, electronic noses need multiple chemical sensors in order to detect different odors: each sensor is able to detect one kind of molecules, so multiple sensors are needed to distinguish multiple types of molecules.

2.2 Artificial Olfaction

"*Did you ever measure a smell? Can you tell whether one smell is just twice strong as another? Can you measure the difference between two kinds of smell and another? It is very obvious that we have very many different kinds of smells, all the way from the odor of violets and roses up to asafetida. But until you can measure their likeness and differences, you can have no science of odor. If you are ambitious to find a new science, measure a smell.*" - Alexander Graham Bell, 1914 [3]

From an early age it was known the odor was something difficult to measure. As Alexander Graham Bell said in 1914, the best way to find a new science was by measuring a smell. In the first decades since Bell has made this observation, no progress was made and consequently no science was found. Finally, in 1982, the first article referring the creation of an odor sensor using three metal oxide semiconductor sensors was published by Persaud and Dodd in Nature journal [4], giving rise to a new science: the science of odor.

The most typically used sensors on electronic noses and their principle of detection can be found in the diagram below, Figure 2.1.

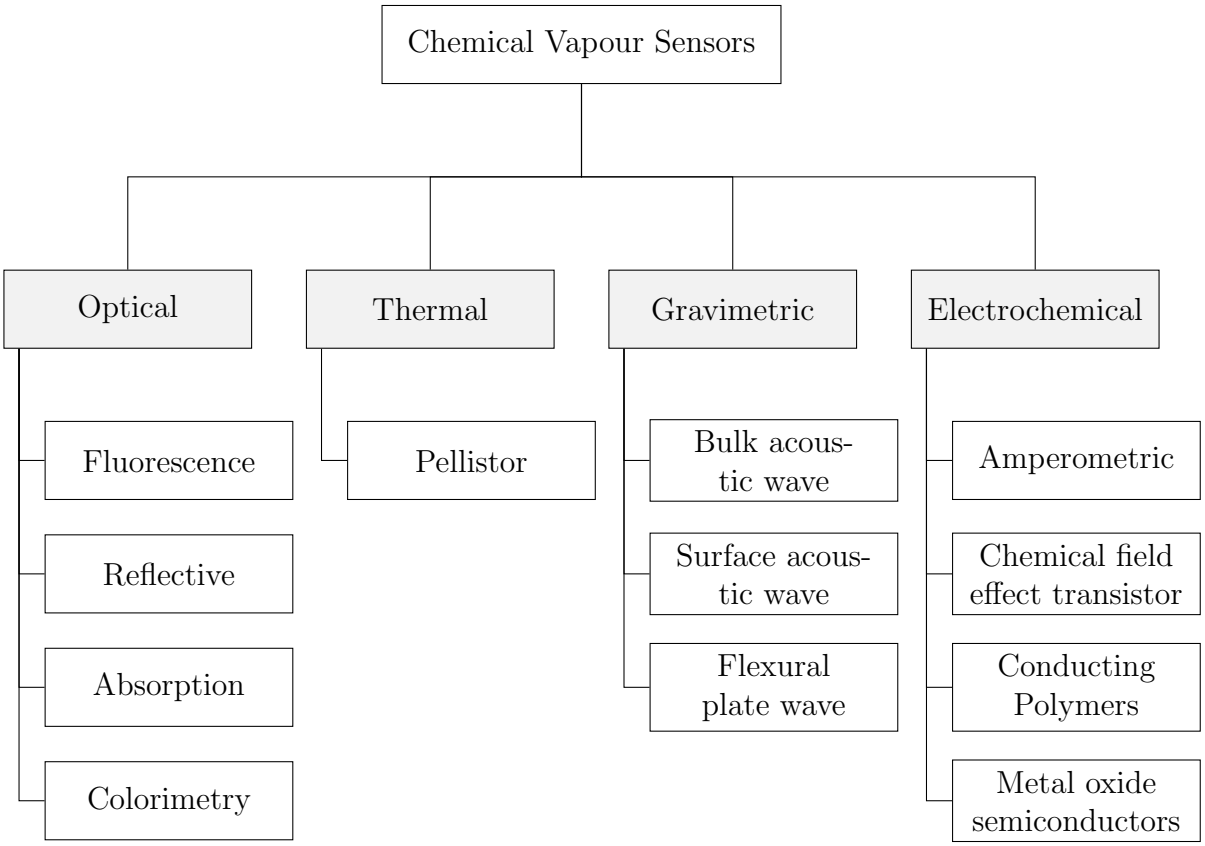

Figure 2.1: Principle of sensors used in electronic nose sensing [5].

Optical Sensors

Optical sensors involve multiple techniques to detect odors, once their optical properties change in the presence of a specific odor. Some of the most used optical properties are: fluorescence, reflection, absorption and colorimetry. Although some progress has been done by Di Natale et al. [6] and Suslick [7] on absorption and colorimetric measurements, fluorescence is the most popular property given its sensitivity, selectivity and versatility [8].

Thermal Sensors

The thermal gas sensors are able to detect gases which are either combustible, through the heat produced by catalytic oxidation of those gases, or which have a significant difference in thermal conductivity when compared to air. Therefore, this type of gas sensors is used only to detect high concentrations of combustible gases. The gas properties, such as its type and concentration, can be defined by analyzing the temperature changes detected. In order to the catalytic reaction occurs, these sensors must be operated at high temperatures, having its high power consumption as a disadvantage.

Gravimetric Sensors

The three types of gravimetric transducers most frequently used in electronic noses are: bulk acoustic wave (BAW), surface acoustic wave (SAW) and, most recently, flexural plate wave (FPW). These sensors are, basically, electromechanical oscillators which propagate acoustic waves through a material composed of a gas sensitive layer (coating layer) and the detection consists of measuring the frequency shift with respect to the mass loading and/or the amplitude shift [9]. This type of gas sensors is usually sensitive, inexpensive and have a fast response time. However, their selectivity is somehow limited by depending on the coating layers used in their development.

Electrochemical Sensors

Electrochemical sensors have been the most widely used in electronic noses. They operate by oxidizing or reducing the surrounding gas at an electrode and producing changes that result in resistance, voltage, or current variations. By measuring these variations, it is possible to estimate the concentration of the target gas, since the sensor's output is a function of the gas concentration. This linear response makes the electrochemical sensors easier to calibrate than the other sensor technologies, whose output must be previously linearized. On the other hand, this type of sensors is not suitable for every gas, such as stable gases like carbon dioxide (CO_2), making them not viable for certain applications.

2.3 Anemometry

Odoriferous molecules can arise in the atmosphere in multiple ways: they can be released directly into the atmosphere in gaseous form, or they may evaporate from a solid or a

liquid. Typically, solids and liquids are used in applications, such as robotics, where the environment is characterized by chemical substances with a specific odor. After evaporation, odor particles tend to diffuse from areas of high concentration to areas of low concentration until equilibrium is reached. In contrast, if there is an airflow near the odor source, given that odoriferous molecules generally have very small molecular masses and are easily drawn by air flows, the diffusion effects will be suppressed by the flow velocity, being the latter responsible for the odor spread. With that said and considering the detection methods used by insects referred in chapter 1, it can be assumed that one of the most effective methods for the odor source localization is to determine the counter-wind direction through anemometry.

Fluid flows have numerous properties that may cause uncertainties and inaccuracies in measuring a flow velocity and, for the same reason, the development of techniques for measuring a flow velocity in fluids has always been a major challenge. Along the years, different methods for flow velocity measurement have been developed and many of them are currently used. Since measuring the speed of a flow is one of the fundamental steps of this work, it is essential to know some of the existing methods in order to analyze their advantages and disadvantages and, finally, to evaluate which is the most suitable method taking into account the objectives of this work.

Floating Particles

Floating particles methods are the most simple, yet effective, methods to measure the flow velocity in fluids (normally liquids). Their principle is based on measuring the velocity of floating particles along a fluid flow using, for instance, computer vision techniques. The particles may be composed of solid material less dense than the fluid, being able to float, or simply be capable of cause some contrast in the fluid. Gas bubbles are commonly used in liquids as floating particles.

Rotating or Oscillating Methods

Rotating methods consists in the transformation of a rotor relative movement, subjected to a liquid or a gas flow. The velocity is easily acquired by digital means, since its calibration depends on the rotation count (usually number of turns per time unit) which is proportional to the flow velocity. Propeller anemometers and cup anemometers are well known examples of this method. When the fluid in study is gaseous, these devices can also measure the flow direction, either by using a vane for orientation or using oscillating fans or structures [10].

The advantages of this type of anemometers are their ease of construction as well as their ease of use. On the other hand, rotating anemometers exhibit low sensitivity and their mechanical wear implies poor durability.

Pressure Differentials

By measuring the pressure at two different points of a flow, its velocity can be obtained based on calculations involving mass and energy conservation concepts. The Bernoulli equation for incompressible fluids is often used to determine the velocity of a fluid:

$$\frac{1}{2}\rho v^2 + \rho g z + p = constant \tag{2.1}$$

where ρ is the density of the fluid, v is the fluid flow velocity, g is the acceleration due to gravity, z is the elevation of the chosen point above a reference plane and p is the pressure at the chosen point. A well known device that makes use of these methods is the pitot tube which measures the fluid pressure p_s (where the velocity, v, is unknown) and the pressure p_0 where the fluid velocity is null. According to Bernoulli's equation (2.1), the velocity of the fluid can be obtained from the following expression:

$$v \approx \left[\frac{2(p_0 - p_s)}{\rho}\right]^{1/2} \tag{2.2}$$

Ultrasonic Methods

Ultrasonic anemometers use pairs of transducers to measure the change in the transmission time of ultrasonic sound waves or the consequent frequency shift, caused by the means of propagation. Measurements from pairs of transducers can be combined to obtain a measurement of velocity in up to 3 dimensional flow, being each pair of transducers responsible for each dimension [11]. Although ultrasonic anemometers provide accurate and reliable wind speed and direction data, their size can compromise their application in mobile robot olfaction.

Laser Doppler Methods

The Laser Doppler Anemometer (LDA) measures the velocity at a point in a flow using light beams. This type of anemometer uses a laser beam that is divided into two beams: one of the beams is kept intact as a reference signal, while the other crosses the fluid in motion.

Then the frequency shift between the scattered light (due to particles flowing along with air) and the reference signal is calculated, thus obtaining the velocity of the fluid. LDAs are known for their non-intrusive measurement, high spatial and temporal resolution, no need for calibration and the ability to measure in reversing flows. Given the high cost and complexity of these devices, their application is practically restricted to aerodynamic tests. Also, since they use light beams, they can only be applied to transparent flows which the light beams can pass through [12].

Thermal Methods

Thermal methods measure the fluid flow velocity through the heat transfer from heated elements to the fluid in motion, giving rise to electrical quantities variations. These methods are often employed for the study of reduced or turbulent flows due to their good sensitivity and reduced thermal inertia, which is assured by using small size heated elements. Hot-wire anemometers are a good example of this method. Thermal anemometers can also be designed to have low power consumption: Sensirion SFM4100 [13] and Honeywell Zephyr [14] are among the sensors with low power consumption, consuming about 12.25 mW and 23 mW, respectively.

2.4 Thermal Anemometry

As referred in the section above, thermal anemometers measure the fluid flow velocity through the changes in heat transferred from a heated element to the flow. Besides the vast number of advantages that thermal anemometers have and taking into consideration their satisfactory performance and their robustness, thermal anemometers can easily be integrated in a wide range of applications/environments. For this reason, this work will focus on the development of an odor source localization device using thermal methods.

The fluid flow velocity can be calculated by measuring electrical quantities variations that depend on the operation mode of the anemometer:

- constant current anemometer (CCA);
- constant voltage anemometer (CVA);
- constant temperature anemometer (CTA);
- constant temperature difference or constant power anemometer (CPA).

Constant current anemometers are based on current source circuits where the current is maintained at a constant value. An example of a constant current source is shown below (Figure 2.2).

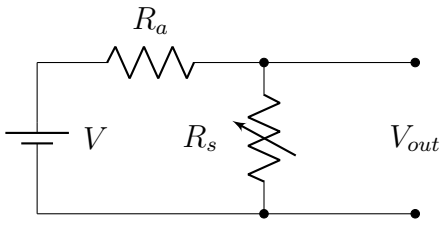

Figure 2.2: Constant current control circuit.

The sensor's current, R_s, is kept constant by ensuring that $R_a \gg R_s$. Then, the fluid velocity can be calculated by measuring the sensor's voltage, V_{out}. In this mode of operation, velocity fluctuations result in temperature changes of the heated element. For this reason, and taking into consideration the heated element's associated thermal inertia, the constant current operation mode presents a poor response to high frequency velocity variations, making it a rarely used operation mode. Other problem with constant current devices is their difficulty to calibrate and use [15].

Similarly to constant current anemometers, constant voltage anemometers principle is based on maintaining the sensor's voltage at a constant value. Figure 2.3 shows a basic constant voltage anemometer circuit using the feedback to maintain the voltage constant.

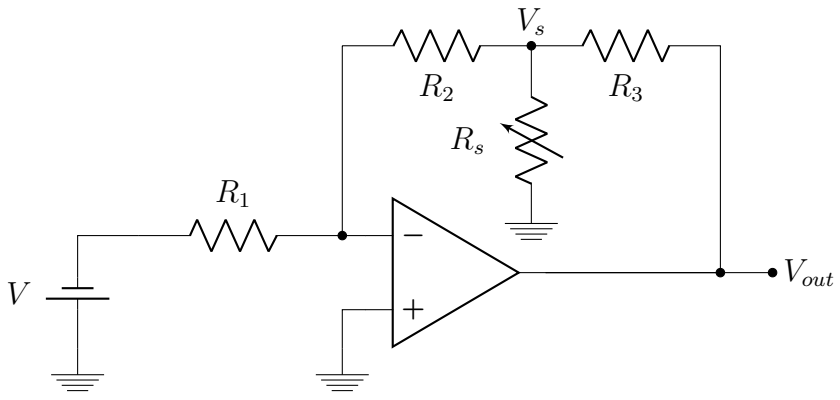

Figure 2.3: Basic constant voltage anemometer circuit.

The circuit shown in Figure 2.3 is an inverting operational amplifier circuit. Analyzing the circuit, it is possible to verify that the sensor's voltage, V_s, is given by $V_s = (R_2/R_1) \cdot V$. NTC (negative temperature coefficient) thermistors are not suitable for constant voltage anemometer configurations, as they degrade when fed at a constant voltage due to the

uncontrolled heating and extreme values of current. Hence, only PTCs (positive temperature coefficient) are used in constant voltage anemometers. Other than that, constant voltage operation mode offers multiples advantages, namely the high frequency response and the large signal-to-noise ratio [16].

The most popular anemometer is the constant temperature anemometer. Its principle of functioning is based on keeping the sensor's resistance at a constant value. Constant temperature anemometers usually use a Wheatstone bridge circuit as shown in Figure 2.4.

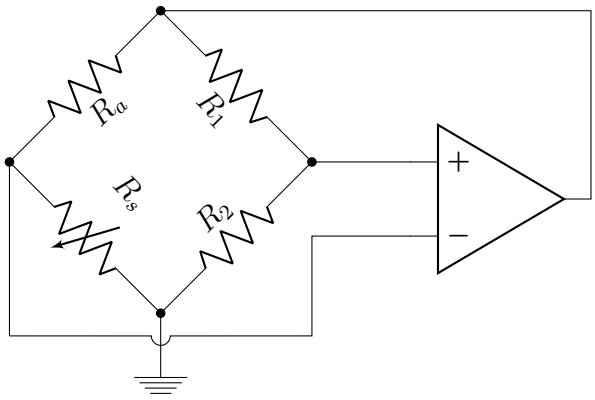

Figure 2.4: Basic constant temperature configuration circuit for PTC thermistors using a Wheatstone bridge.

Considering that the operational amplifier has an infinite gain, it can be assumed that the bridge is balanced. In other words, the input voltages at the operational amplifier tend to be equal. With that being said, the resistance R_s of the sensor can be obtained by knowing the relation between the Wheatstone bridge's resistors:

$$\frac{R_a}{R_s} = \frac{R_1}{R_2} \Leftrightarrow R_s = \frac{R_2}{R_1} R_a \tag{2.3}$$

When a temperature change occurs in the sensor, the input voltages at the operational amplifier will not be equal, and the difference between them (voltage error) will be amplified and fed back to the top of the bridge, until the bridge is in balance again.

The configuration shown in Figure 2.4 is for PTC thermistors. In order to use NTC thermistors, the configuration needs to be readjusted: the inputs of the operational amplifier or the resistors R_s and R_a must be interchanged.

This type of device is particularly suitable for the measurement of flows with very fast fluctuations at a certain point, given its high spatial and temporal resolution when using heated elements with reduced dimensions. This configuration also assures the absence of thermal inertia problems, as there are no considerable changes in the sensor's temperature.

Finally, the last operation mode is the constant temperature difference (constant power mode). It is identical to the constant temperature operation mode, however, in constant power anemometers, the difference between the sensor's temperature and the environment temperature is kept constant, that is, $T_s - T_{env} = const.$ For PTC thermistors, assuming that the sensor's response is linear, a similar configuration circuit to the one shown in Figure 2.4 can be used for compensating temperature fluctuations, being necessary to change R_2 by a thermistor with the same temperature coefficient as the sensor. If the sensor's response is non-linear, a different and more complex approach is required.

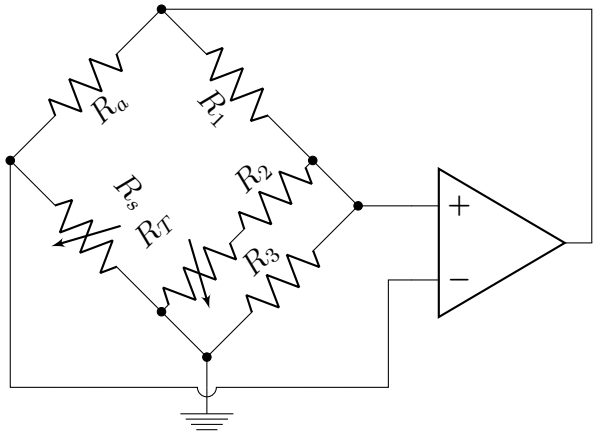

Figure 2.5: Constant power configuration circuit [15].

Figure 2.5 shows a circuit diagram generally used on constant power anemometers. The values of R_2 and R_3 are chosen such that the Equation (2.4) is valid for the entire operating temperature range of the sensor.

$$\frac{R_s(T)}{R_a} = \frac{R'_T(T)}{R_1} \Leftrightarrow \frac{R_s(T)}{R_a} = \frac{[R_T(T) + R_2]R_3}{[R_T(T) + R_2 + R_3]} \cdot \frac{1}{R_1} \tag{2.4}$$

Due to its temperature compensation, the constant power operation mode is the most straightforward mode for calculating the fluid flow velocity, as shown in the next chapter.

2.5 State of the Art

Although odor detection sensors have already been briefly presented, this sections intends for a more detailed analysis on what has been done so far in this area.

2.5.1 Directional Anemometers

Prior to the work reported in this dissertation, a sensor based on thermal methods was developed in the University of Coimbra to address the same problem [17]. The sensor was based on a constant temperature method of operation and used multiple NTC thermistors disposed in a triangular structure to measure both the airflow velocity and direction. It presented satisfactory results when measuring flow velocities above 0.1 m/s. However, the anemometer structural design originated ambiguities when obtaining the direction of the airflow.

Thermal methods are also frequently based on MEMS (Micro-Electro-Mechanical Systems) technology, since they usually have a very low energy consumption, as it was developed in the University of Freiburg. The developed device consists in a two-dimensional anemometer using five highly sensitive amorphous germanium thermistors, where one of the thermistors, the heater element, was placed at the center of the device and the remaining thermistors, the sensing elements, were placed in such a manner that they would form a square centered in the heater element. The sensor has proved to be very efficient and accurate, having a maximum angle error of 3.5° and a power consumption of 0.177 mW_{rms} when detecting flow velocities below 1 cm/s [18].

Thermal anemometers are also known for their high accuracy and precision. There is, in fact, a device based on three MEMS hot-film sensors placed around a circular structure which is capable of measuring the wind speed with an accuracy of 3.6% RMS (root mean square) error in a range of 0.1-10 m/s, and the wind direction with an accuracy of 1.20° (RMS error), considering a scale of 360 degrees [19].

2.5.2 Odor Compasses

Multiple articles and products can be found using multiple MOS gas sensors combined in such a manner that it is possible to obtain the direction of an odor's origin. One of them is a device developed in the Tianjin University which requires three MOS sensors of the same type (not calibrated) placed in a triangular disposition and uses a scale-space method to obtain multitime-scale information, allowing for a precise odor tracking [20]. This method also uses relative output information from the sensors, thus eliminating the influence of the sensors drift.

Another work, developed in Tokyo Institute of Technology, had as its objective to build a three-dimensional odor compass based on the method used by male silkworm moths to

track sexual pheromones so they could locate their female counterpart. It consisted of a device with four MOS gas sensors separated by acrylic plates and a small fan to push air to the sensors [21], simulating the effect caused by the silkworm moths' vibrating wings. The odor direction could then be obtained by rotating the compass head within two degrees of freedom until the responses of the MOS sensors along the horizontal and vertical directions were balanced.

Last but not least, an olfactory system for odor-plume tracking and localization was designed in the University of Coimbra with the purpose of allowing for an autonomous search of odor sources in outdoor environments using a mobile robot [22]. The system consisted of three intelligent modules: two gas sensing nostrils and a directional thermal anemometer, and the localization of a specific odor source was then estimated by merging the information gathered from the sensing modules with the spatio-temporal localization of the mobile robot. The olfactory system developed presented satisfactory results, demonstrating that combining a directional thermal anemometer with electronic noses is a viable option regarding the odor source's localization.

3 Materials and Methods

3.1 Fluid Flow Measurement

The temperature of a sensing element at any instant of time depends on the rate of heat transfer. Furthermore, heat transfer in an element is the result of three processes: radiation, conduction and convection [23].

Thermal radiation results from the emission of electromagnetic waves. It consists in the result of random movements of atoms and molecules in matter. For reduced temperature differences, thermal radiation is not significant and can thus be neglected [24].

Conduction transfers heat through direct molecular collisions, being the main heat transfer mechanism inside solids. In thermal anemometers, conduction occurs due to losses in the supports of the sensing elements, being this a factor to be taken into consideration on the sensor's design.

Finally, convection is the main heat transfer mechanism between the fluid and the sensing element immersed in the fluid. It consists in the transfer of thermal energy by fluids in motion due to random molecular motion (diffusion) and macroscopic motion of the fluid. Convective heat transfer may be divided into two types:

- Natural convection: the fluid motion is caused by natural means, namely buoyancy forces that result from the density variations due to temperature variations in the fluid;
- Forced convection: the fluid motion is caused by external means such as a pump or a fan, being forced to flow over the surface creating an artificially induced convection current.

Convective heat transfer is described by Newton's law of cooling. It relates the rate of heat loss with the difference between the heated element temperature and the environment temperature. The rate of convective heat transfer is given in the form of a differential equation:

$$\frac{dQ_R}{dt} = \dot{Q_R} = P_T = k(T_s - T_{env}), \text{ with } k = h \cdot A \tag{3.1}$$

where Q_R is the thermal energy released to the environment $[J]$, P_T is the thermal power dissipated $[W]$, k is the dissipation factor $[W/K]$, T_s is the temperature of the heated element $[K]$, T_{env} is the temperature of the environment $[K]$, A is the heat transfer surface area $[m^2]$ and h is the heat transfer coefficient $[W/m^2.K]$.

In 1914, King verified that the heat transfer coefficient, h, is a function of the fluid flow velocity, v_f, deriving a solution known as King's law for hot wires:

$$h = a + b \cdot (v_f)^c \tag{3.2}$$

where a, b and c are coefficients obtained through calibration ($c \approx 0.5$).

When the thermodynamic equilibrium is satisfied, the rate of energy supplied ($\dot{Q}$) shall be equal to the sum of the rate of energy stored by the device ($\dot{Q_S}$) and the rate of energy released to the environment ($\dot{Q_R}$).

$$\frac{dQ}{dt} = \frac{dQ_S}{dt} + \frac{dQ_R}{dt} \tag{3.3}$$

The rate of energy released to the environment, $\dot{Q_R}$, can be calculated as defined previously in Equation (3.1) and the rate of energy stored by the device, $\dot{Q_S}$, is given by:

$$\frac{dQ_S}{dt} = \frac{Q}{\Delta T}\frac{dT_s}{dt} = C\frac{dT_s}{dt} \tag{3.4}$$

In the equilibrium state ($\frac{dT_s}{dt} = 0$), the term $\dot{Q_S}$ is null, thus the rate of energy supplied, $\dot{Q}$, is equal to the rate of energy released to the environment, $\dot{Q_R}$. Since the heated element is a resistor, the heat is generated by Joule's effect and the thermal power dissipated is equal to the electric power supplied.

$$\frac{dQ_R}{dt} = P_E = VI = RI^2 = \frac{V^2}{R} \tag{3.5}$$

Thus, by using the Equations (3.1), (3.2) and (3.5), the expression relating the fluid flow velocity, v_f, with the electrical power, P_E, can be obtained:

$$P_E = \frac{V_R^2}{R_T} = (a + b \cdot (v_f)^c) \cdot A \cdot (T - T_{env}) \tag{3.6}$$

By manipulating Equation (3.6), the fluid flow velocity may be finally calculated:

$$v_f = \left[\frac{V_R^2}{R_T \cdot A \cdot (T - T_{env}) \cdot b} - \frac{a}{b} \right]^{\frac{1}{c}} \tag{3.7}$$

where V_R and R_T are, respectively, the voltage and the resistance of the heated element at temperature T. When using a constant temperature difference operation mode, the term $(T - T_{env})$ will be kept constant and, therefore, Equation (3.7) can be written as follows:

$$v_f = (k_1 + k_2 \cdot V_R)^{\frac{2}{c}} \tag{3.8}$$

where k_1, k_2 and c are coefficients obtained through calibration ($c \approx 0.5$).

3.1.1 Resistance/Temperature Characteristic

The heated element used in thermal anemometers is a thermistor - resistor whose resistance is dependent on the temperature. A thermistor can be used either to measure the temperature or to be heated to a certain temperature through Joule's effect, similarly to its use in anemometry. Thus, the resistance/temperature characteristic of thermistors is an important subject when addressing thermal anemometers.

A thermistor may have a positive temperature coefficient (PTC), causing a resistance increase as temperature increases, or a negative temperature coefficient (NTC), making its resistance to decrease as temperature increases.

$$R_T = a + bT \tag{3.9}$$

Although there exists PTC thermistors with an almost linear response as shown in Equation (3.9), overall, thermistors have an exponential resistance/temperature characteristic as specified in Equation (3.10), so the linear approximation that characterizes the resistance of a thermistor as a function of temperature is a good approximation for small temperature ranges, leading to a high error for wider ranges.

$$R_T = R_{25} \exp\left\{ \beta \left(\frac{1}{T} - \frac{1}{T_{25}} \right) \right\} \tag{3.10}$$

For accurate temperature measurements, the resistance/temperature curve of the thermistor should be described in more detail. The Steinhart-Hart equation (3.11) is a third-order

method widely used, proving to be one of the most accurate methods.

$$\frac{1}{T} = a + b\ln(R_T) + c\ln^2(R_T) + d\ln^3(R_T) \tag{3.11}$$

where T is the temperature (K), R_T is the resistance at temperature T (Ω) and a, b, c and d are the Steinhart–Hart coefficients which describe the type and model of thermistor. The term $[\ln(R)]^2$ is frequently neglected given its low contribution when compared to other terms of the equation. To calculate the coefficients of Steinhart–Hart, four operating points must be known, where R_1, R_2, R_3 and R_4 are the resistance values of the thermistor at the temperatures T_1, T_2, T_3 and T_4, respectively:

$$\begin{bmatrix} 1 & \ln(R_1) & \ln^2(R_1) & \ln^3(R_1) \\ 1 & \ln(R_2) & \ln^2(R_2) & \ln^3(R_2) \\ 1 & \ln(R_3) & \ln^2(R_3) & \ln^3(R_3) \\ 1 & \ln(R_4) & \ln^2(R_4) & \ln^3(R_4) \end{bmatrix} \begin{bmatrix} a \\ b \\ c \\ d \end{bmatrix} = \begin{bmatrix} 1/T_1 \\ 1/T_2 \\ 1/T_3 \\ 1/T_4 \end{bmatrix} \tag{3.12}$$

3.2 Metal Oxide Sensors

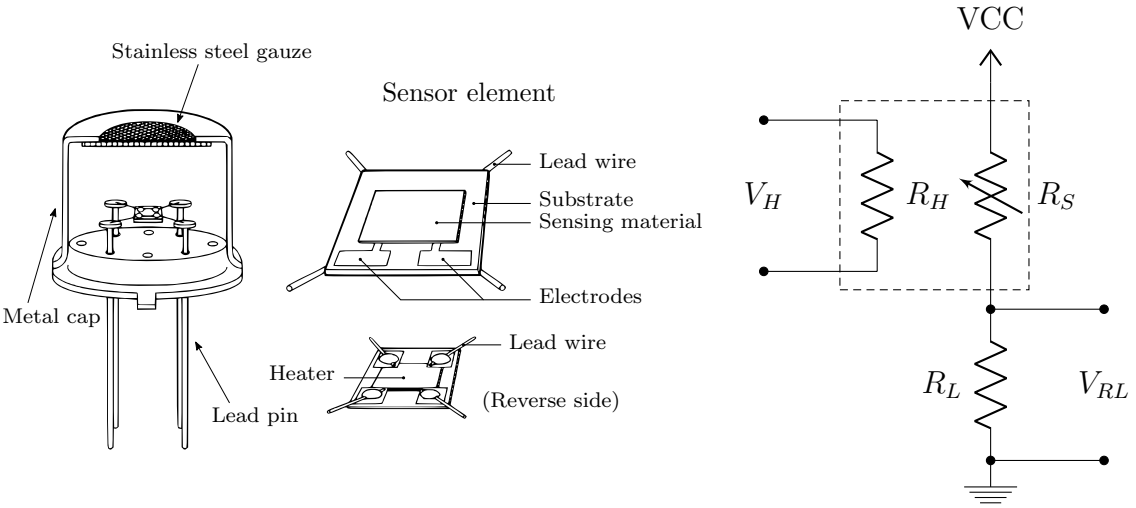

Figure 3.1: Structure of a metal oxide gas sensor and its measuring circuit.

Metal oxide sensors were already introduced in the previous chapter. They are electrochemical sensors, composed by a semiconductor layer (usually, tin dioxide - SnO_2), a metal resistor for heating purposes (R_H) and an insulating layer between the heating resistor and the semiconductor layer. When at ambient temperature, the semiconductor material is in the non-doped state, however, when the metal resistor heats the semiconductor material at

an elevated temperature, the material adsorbs oxygen molecules (O_2), which will attract free electrons previously released by thermal means. Thus, the surface-formed potential inhibits the flow of electrons, increasing the resistance of the sensor (R_S) in clean air. When the exposure of the sensor to combustible or reducing gases occurs, the oxidation reaction of the gas with adsorbed oxygen molecules takes place and the surface-formed potential decreases, allowing the flow of electrons and, consequently, the resistance of the sensor decreases. The relation between the sensor's resistance, R_S, and the gas concentration is shown as follows:

$$R_S \approx R_0 \cdot kC^{\alpha} \tag{3.13}$$

where R_S is the measured resistance, R_0 is the measured resistance when no gas is detected, C is the gas concentration and k and α are sensor constants.

3.2.1 Detecting Multiple Odors

MOX sensors are usually not very selective, being able to detect a small range of odors. Different techniques have been proposed regarding the selectivity enhancement of MOX sensors, among which the thermal modulation of the sensor's pallet has been the most popular method. Therefore, one can assume that the response of the MOX sensor is also temperature dependent and, through the temperature variation, by applying different voltages and waveforms to the heating resistor, R_H, it becomes possible to extract sufficient information in order to identify the gas to be determined, enabling the detection for multiple gases [25].

3.2.2 Degradation of MOX Sensors

One of the known problems of MOX sensors is their long term instability. When a MOX sensor is exposed to a gas for a long time, its response becomes different due to poisoning by irreversible adsorption of contaminants, changing the sensor's properties, such as selectivity and sensitivity, thus affecting the parameters R_0, k and α. In applications were these properties are desired, the sensor drift must be identified and then compensated. One of the methods to compensate the sensor drift consists in predicting the change of the sensor parameters based on their derivatives [26]:

$$\hat{R}_0(t) = R_0 + t \cdot \frac{R_0(t_1) - R_0(t_2)}{t_1 - t_2} \tag{3.14}$$

Finally, the parameters k and α may be calculated in an analogous way.

4 Odor Compass

After referring the theoretical fundamentals which support the sensor's functioning, the development of the sensor will be discussed in detail in this chapter. Three topics will be addressed:

- Sensor Structure;
- Electronics;
- Processing.

4.1 Sensor Structure

The sensor structure is one of the fundamental parts regarding the development of an odor compass. Therefore, multiple structures will be studied, so their advantages and disadvantages can be analyzed.

In order to measure the air flow direction, the sensor shall have a structure capable of changing the flow properties around it as a function of its orientation. Taking into account that the main objective is to obtain a measurement of velocity in two-dimensional flow, at least three sensing points must be taken into consideration. Thus, the structure of the sensor shall be such that it will be possible to measure the flow velocity in, at least, three different points.

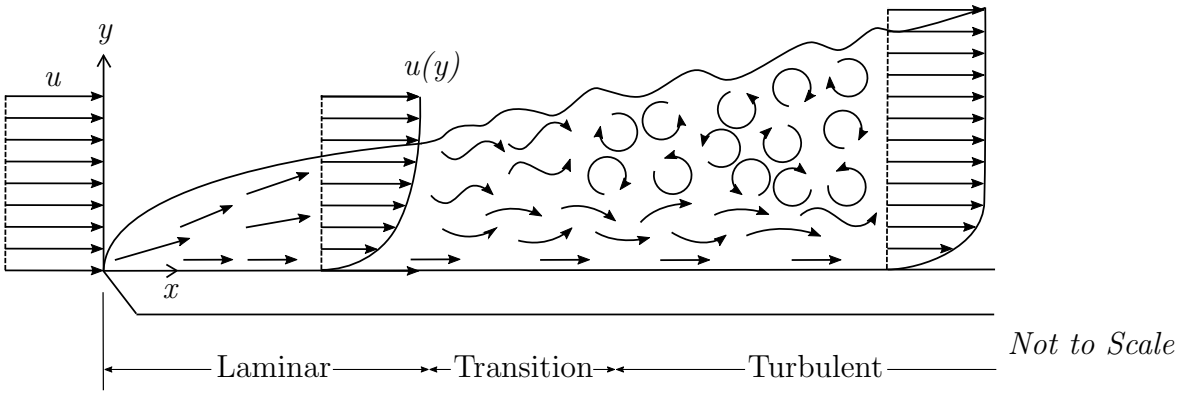

Figure 4.1: Flow of a fluid over a flat plate [27].

To study the fluid flow past a structure it is important to know the region which better characterizes the flow. Thus, the flow of a fluid over a flat plate, as shown in Figure 4.1, can be characterized by taking into consideration three different regions:

- Laminar region, where the flow behavior is very predictable;
- Transition region, where small disturbances/oscillations begin to develop;
- Turbulent region, where the disturbances are such that the flow behavior becomes unstable and unpredictable.

In the boundary layer flow over a flat plate, after a certain length, a laminar flow will begin its transition to turbulent flow, eventually becoming fully turbulent and unstable. The transition region can be defined through the Reynolds number and, considering the flow over a flat plate, such transition occurs when $Re \approx 5 \times 10^5$ [28]. The Reynolds number can then be calculated as follows:

$$Re = \frac{\rho v L}{\mu} \tag{4.1}$$

where ρ is the fluid density, v is the undisturbed flow velocity, L is the distance from the leading edge (characteristic length) and μ is the fluid dynamic viscosity.

Since the fluid in study is the air, it can be assumed that the fluid is *Newtonian*, meaning that its viscosity is constant with respect to shear rate. Additionally, although the fluid density can vary due to pressure changes, it will be considered constant as the Mach number is less than 0.3, indicating that the fluid is only weakly compressible for the case under study. Thus, taking into consideration the previous assumptions, the maximum distance that a flat plate can have in order to guarantee a laminar flow can be easily calculated. In this case, since the purpose of this work is to develop a small size sensor with a volume in the order of tens of cubic centimeters capable to measure low airflow velocities, it can be considered that $Re \ll 5 \times 10^5$ and, therefore, the surrounding flow will be laminar for reduced angles of attack, thus being possible to predict the flow behavior by solving the steady-state Navier-Stokes differential equations responsible for predicting parameters such as the flow velocity and pressure.

Another aspect to take into consideration is the turbulence originated by the flow past the structure used to measure the airflow orientation. In a general way, the turbulence and consequent error originated by the flow past the structure can be quantified through the drag (C_D) and lift (C_L) coefficients:

$$C_D = \frac{2F_D}{\rho v^2 S} \qquad C_L = \frac{2F_L}{\rho v^2 S} \tag{4.2}$$

where F_D and F_L are the drag and lift forces, respectively, ρ is the fluid density, v is the undisturbed flow velocity and S is the surface area. With that said, one of the objectives of this work is also to design a structure whose drag and lift coefficients are as low as possible in order to minimize the error introduced by turbulence.

Therefore, a set of simulations considering a laminar flow were made using COMSOL Multiphysics, which is a software able to solve steady-state and transient laminar problems. To note that the following simulations were made considering the existence of two dimensions only, which is similar to performing three-dimensional simulations considering an infinite height structure.

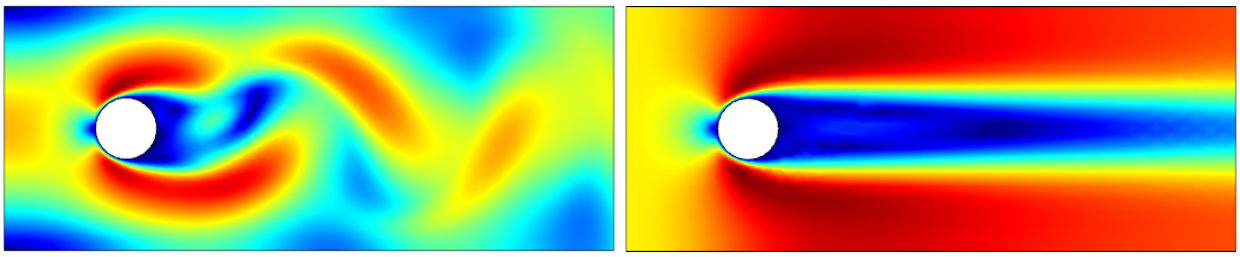

(a) Time dependent simulation (b) Stationary simulation

Figure 4.2: Simulation of laminar flow past a cylinder.

A cylindrical structure allows a solution with a minimum number of thermistors required for flow direction measurement, minimizing the power consumption of the sensor. The resulting disturbances from the flow past the cylindrical structure are always similar, regardless of the flow direction or the orientation of the sensor, as shown in Figure 4.2. Also, cylindrical structures are those with a lower drag coefficient, being the less affected by turbulence. Despite this being a major advantage of cylindrical structures, it is difficult to implement a small size solution with a cylindrical structure, since there are no flat surfaces.

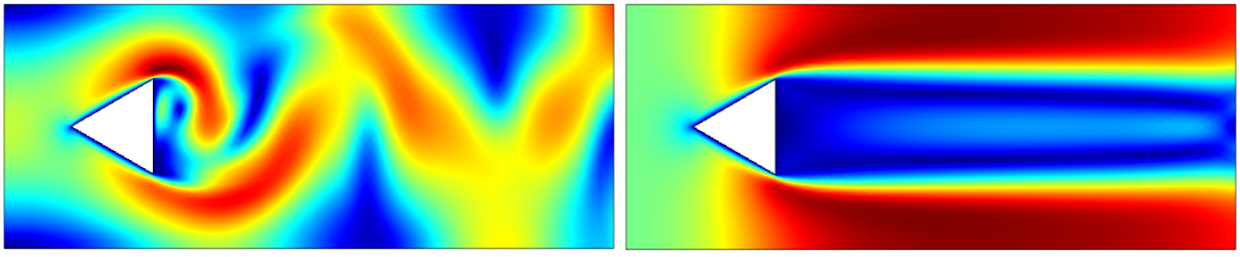

(a) Time dependent simulation (b) Stationary simulation

Figure 4.3: Simulation of laminar flow past a triangular cylinder.

Similarly to cylindrical structures, triangular structures also require the minimum number of sensing points to measure the flow direction. Due to the existence of flat surfaces, it becomes possible to implement a reduced dimension solution through the use of multiple

printed circuit boards (PCBs). However, in this type of structure, the resulting disturbances from the flow past depend on the flow direction, since the angle of incidence changes according to the orientation of the structure. Also, the lift and drag coefficients have shown to be superior than the coefficients of the cylindrical structure.

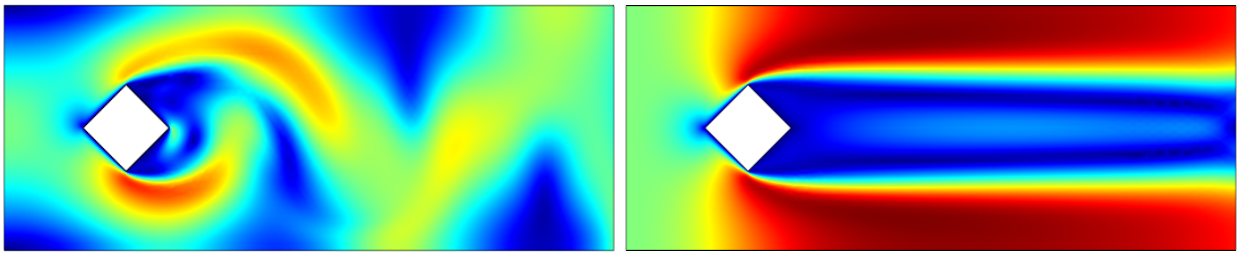

(a) Time dependent simulation (b) Stationary simulation

Figure 4.4: Simulation of laminar flow past a cube.

The cubic structure is quite identical to the triangular structure, however, it requires one more thermistor than triangular and cylindrical structures, due to the existence of four surfaces for measuring the flow direction. As a consequence, this solution presents a highest power consumption. Although it is the easiest solution to implement, since the surfaces are perpendicular to each other, the addition of a face in comparison with the triangular solution does not introduce any relevant advantages.

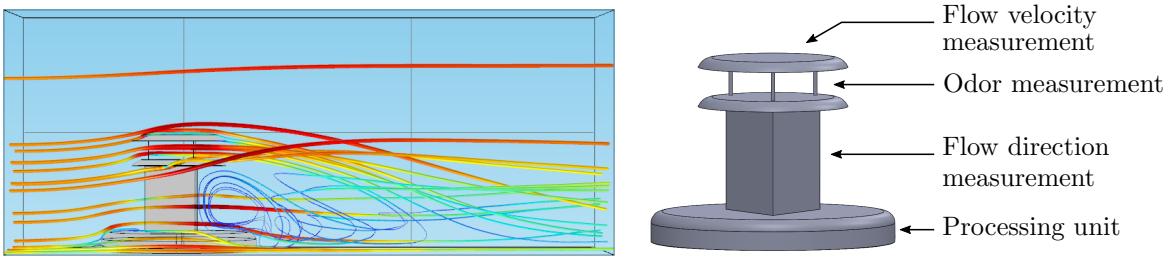

(a) Stationary simulation (b) Structure of the developed sensor.

Figure 4.5: Simulation of laminar flow past the designed structure.

Given the ease of construction of a triangular structure and its advantages when compared to cubic and cylindrical structures, the developed sensor is based on triangular structures. Although triangular structures are more affected by turbulence when compared to cylindrical structures, it has been proved by several studies (Carassale et al. [29], Zhdan et al. [30] and Nidhul [31]) that by rounding the structure corners, one can promote the reattachment of the flow on the lateral faces. Rounding the structure corners also results in a decrease of the pressure variation in the near wake region and hence the flow separation is delayed.

As shown in Figure 4.5b, the developed sensor can be divided into four fundamental parts: the base of the sensor, where the processing of the transducer signals occurs, the triangular structure itself, the bottom plate, where a MOX sensor is located, and the top plate, where the flow velocity and the ambient temperature can be measured. In order for the sensor to have a similar structure to the one shown in Figure 4.5, multiple PCBs were designed so they could interconnect with each other and fit in a plastic frame working as the "chassis" of the sensor. The three-dimensional simulation made considering the real structure of the sensor shown in 4.5a shows that the boundary layer flow is mostly laminar, demonstrating that it is possible to measure the airflow direction with a reduced error introduced by turbulence. As expected, the rounded cylinders (circular plates) played an essential role on the structure of the developed sensor by promoting the flow reattachment and reducing the turbulence effects. Also, the flow velocity in the near wake region has shown to be reduced, thus delaying the flow separation from the structure.

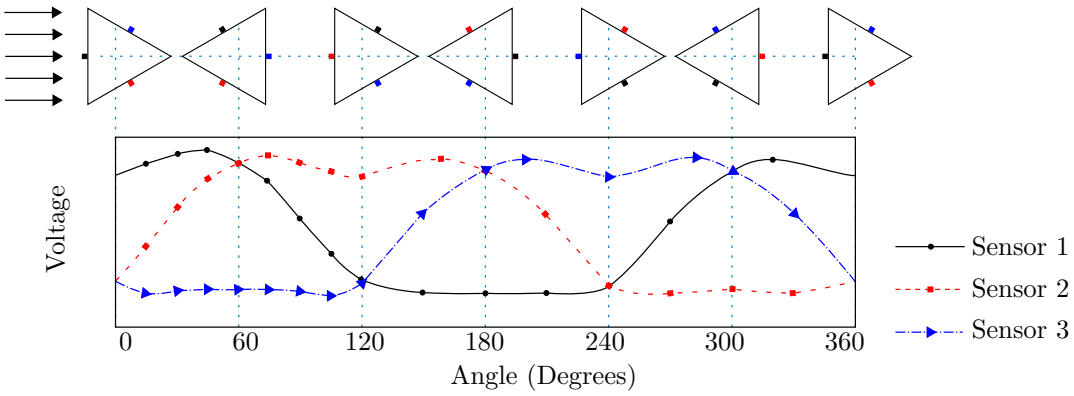

Figure 4.6: Expected response of the three sensing points on a triangular structure [19].

Figure 4.6 shows the expected response of the three sensing points located in the center of each face of the triangular structure. Each time one of the vertices points in the opposite direction of the flow, the flow velocity measured by the sensing points closer to the vertex is maximum. Thus, in a complete turn of the structure, considering the presence of a flow with constant velocity, each sensing point should reach its maximum value two times with a 120 degree offset from each other.

4.1.1 Influence of the PCB's Copper Tracks

Copper is an excellent thermal conductor (thermal conductivity of 400 $W/m.K$, approximately) so, it is important to study the influence that the copper tracks of the PCB exert on the heat dissipation of the heated element. The set of processes involving heat transfer

between solids and fluids due to thermal interaction between them is often described as conjugate heat transfer. A typical example where conjugate heat transfer dominates is the cooling of a solid object by the passage of an airflow in which the solid is immersed. Conjugate heat transfer problems can also be solved by COMSOL Multiphysics and, therefore, it will be the software used to study the heat transfer between the heated elements of the developed sensor and the airflow surrounding the sensor.

Multiple simulations of the airflow past the heated element at a temperature of $60°C$ were made considering two different dispositions: a PCB with the copper trace on top and a PCB with the copper trace on bottom. Thus, considering the conjugate heat transfer, an environment temperature of $20°C$, a flow velocity of 1 m/s and a SMD thermistor with a 0603 package (.06 x .03 inches) as shown in Figure 4.8, the following results were obtained:

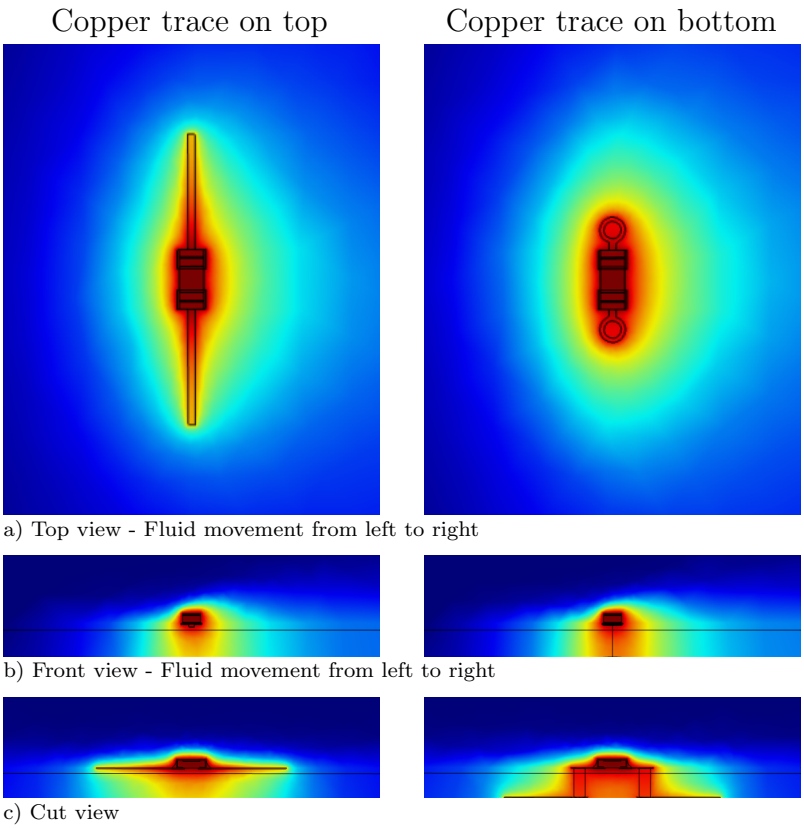

Figure 4.7: Simulation of laminar flow past the heated element.

By analyzing Figure 4.7, it is possible to verify that, although the copper track on bottom presents better results, in both cases the copper tracks dissipate a considerable amount of heat, resulting in the increase of the sensor's power consumption. On the other hand, considering the structure adopted in the previous section and a steady state situation, copper tracks on bottom of the PCBs will not result in significant heat losses since the interior part of the structure will not be subject to airflows.

Along with the simulations shown in Figure 4.7, multiple simulations were made considering different SMD packages (1206, 0805, 0603 and 0402) with the purpose of analyzing the impact that the size of the heated element would have in the sensor's power consumption and also in the heat transfer between the heated element and the air. For the same temperature range, the larger size thermistor (1206) has proved to be more sensitive to fluctuations of the flow velocity despite the higher power consumption. However, the fact that a smaller thermistor can reach higher temperatures considering the same power consumption makes both package sizes equally sensitive. On the other hand, it has been noted that the smaller the size of the heated element, the greater the ratio between the heat dissipated by the copper tracks and the heat produced by the thermal element, demonstrating that thermistors with a very small size are not advantageous at all since the copper tracks act as heat sinks. A solution to this problem consists in producing a printed circuit board whose copper tracks are as thin as possible, decreasing the available copper area, and whose composite material has a reduced thermal conductivity.

4.2 Electronics

Electronics is a branch of Physics that studies the flow and control of electrons and their behavior in active and passive electrical components that, when interconnected in a closed loop, form an electrical circuit. Since the 18th century this area has been constantly evolving, being essential nowadays, especially after the discovery of the transistor in 1947.

Such as the sensor structure, electronics is a fundamental part regarding the development of the odor compass, being crucial in temperature measurement, odor detection and heating the thermistors. In other words, electronics is responsible for interpreting data from the real world through the use of transducers. Then, using converters, such as analog-to-digital converters (ADCs), the data can be transformed into both readable and intelligible data and then analyzed by the human user.

4.2.1 Self-Heating

The self-heating process is essential when measuring the airflow velocity. So, the choice of the heated element should be made carefully, such as the mode of operation of the anemometer. The most advantageous mode of operation is the constant power mode, however, some precautions, as the choice of the temperature compensation method, are required for its

implementation.

As stated in chapter 2, a high thermal inertia is a recurring problem regarding this process and needs to be taken into consideration. Simply put, the lower the thermal inertia, the better the response to the variation of the airflow velocity. The thermal inertia of a material is defined as the square root of the product between the material's thermal conductivity and the volumetric heat capacity, which is directly proportional to the material's heat capacity, leading to:

$$C = c \cdot m = \frac{Q}{\Delta T} \Leftrightarrow \Delta T = \frac{Q}{c \cdot m} \tag{4.3}$$

where C is the heat capacity, c is the specific heat capacity, m is the mass of the body, Q is the amount of thermal energy and ΔT is the resulting temperature change. Through the analysis of the Equation (4.3), it can be concluded that the resulting temperature change (ΔT) increases with the raise of the amount of thermal energy, the decrement of the specific heat capacity or the decrement of the mass of the body. Since the purpose of this work does not concerns the construction of the heated elements, properties such as the specific heat capacity are extremely difficult to change. Therefore, to ensure a thermal inertia as small as possible, it is necessary to use heated elements with the lowest possible mass. Nowadays, there are several electronic components, known as surface-mount devices (SMDs), which can be mounted directly onto PCBs, thus allowing the use of elements of reduced dimensions and with a low dissipation factor, minimizing the thermal inertia problem.

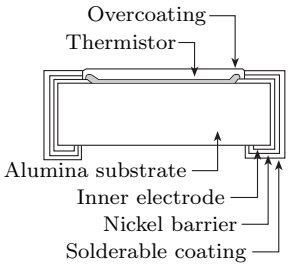

Figure 4.8: Nickel thin film linear thermistors construction.

One other point to keep in mind is the temperature coefficient of the thermistor used as heated element. Typically, NTC thermistors have a negative exponential curve and, to avoid their degradation due to high values of current when used as heated elements, a thermistor with a high resistance at $25°C$ (R_{25}) is required. Hence, a disadvantage of using NTC thermistors is the need of a high operating voltage to start the self-heating process. On the other hand, PTC thermistors may have an exponential or linear curve and, therefore, a thermistor with a low resistance at $25°C$ can be used as heated element, needing a low operation voltage to start the self-heating process.

The Vishay TFPT series is ideal for this application. These are SMD nickel thin film linear thermistors (Figure 4.8) with a positive temperature coefficient, reduced dimensions ($1.55 \times 0.8 \times 0.45\ mm$), a weight of, approximately, 2 mg, a resistance value at $25°C$ of

100 Ω and a low dissipation factor, $\delta = 1.8\ mW/K$, allowing a low power consumption and assuring a reduced thermal inertia.

After choosing the heated element, there remains the development of a solution allowing the controlled self-heating of the sensing elements. Figure 4.9 shows the electrical circuit used to heat one of the thermistors in a constant power operation mode.

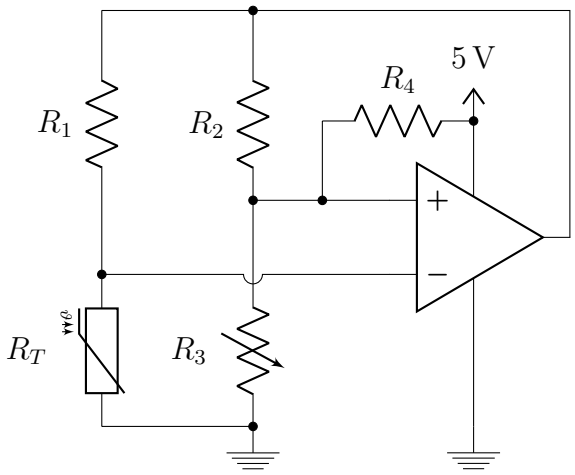

Figure 4.9: Electric circuit for the self-heating process.

The electrical circuit shown above depends on the feedback to maintain the temperature difference between the heated element and the environment at a constant value, assuring a constant power operation mode. It is based on the comparison of two voltages: the voltage at the non-inverting input of the operational amplifier, V_+, and the voltage at the inverting input, V_-. When $V_+ \neq V_-$, the Wheatstone bridge is assumed to be unbalanced and the feedback loop is responsible for balancing it by feeding (or not) the top of the bridge. In other words, assuming an initial state in which the bridge is balanced, when an air flow passes through the PTC thermistor, the thermistor will cool down, resulting in the decrease of both its resistance and the voltage V_- such that $V_- < V_+$. Hence, the output voltage of the operational amplifier will be greater than zero, resulting in the heating of the thermistor until the voltages V_- and V_+ are equal again. On the other hand, if the ambient temperature decreases (decrease of R_3 resistance, as further explained) or, for some reason, the thermistor heats up more than expected such that $V_- > V_+$, the output voltage of the operational amplifier will be equal to zero so that the thermistor cools down until the bridge is balanced again. This procedure is only possible by using an operational amplifier with wide bandwidth, a high open loop gain and rail-to-rail input and output. Typically, the driving between the operational amplifier and the top of the bridge is made using a transistor acting as a current amplifying device. In this case, it is done in a direct manner

so, the output current from the operational amplifier is also an important characteristic to take into consideration. The AD8531 from Analog Devices is a single-supply amplifier with all the mentioned characteristics featuring a 250 mA output drive current, making it an excellent option for this application.

By using a variable resistor controlled by software in R_3 it becomes possible to compensate the temperature in a hybrid way: using software to obtain the ambient temperature and then set the desired resistance value in R_3; and using hardware to, through feedback, automatically heat the thermistor R_T and maintain its resistance at a constant value as explained above. AD527x digital rheostats from Analog Devices are an excellent option for this application due to their low resistor tolerance error of 1%, high resolution (256 or 1024 positions) and linear response.

$$R_3(T_{env}) = R_2 \cdot \frac{R_T(T_{env} + \Delta T)}{R_1} \tag{4.4}$$

Equation 4.4 shows the digital rheostat resistance value, R_3, as a function of the environment temperature, T_{env}, where ΔT is the desired temperature difference between the heated element and the environment, R_1 is a resistor such that $R_1 \ll R_T$ so the thermistor can heat up and R_2 depends on the temperature range desired for the heated element. This temperature compensation method requires a precise resistance/temperature curve of the thermistor, $R_T(T)$, which can be obtained by using the concepts described in section 3.1.1. In this case, the intended temperature range is $[25 - \alpha,\ 25 + \alpha]$ $(^\circ C)$, with $\alpha \propto \max(R_3)$. Therefore, R_2 can be obtained through Equation (4.5).

$$R_2 = \frac{R_1}{R_T(25^\circ C)} \cdot \frac{\max(R_3)}{2} \tag{4.5}$$

Typically, the initial state of this type of circuits is unknown due to the same voltage value at the inverting and non-inverting inputs of the operational amplifier ($V_+ - V_- = 0$) so, a transition from "no power" to "power" may not be enough to start the self-heating process. To guarantee a known initial state, a resistor (R_4) must be placed between the non-inverting input of the operational amplifier and the power supply, adding a voltage offset to the non-inverting input. Note that, in order to minimize the error introduced by the voltage offset, R_4 must have a resistance value as high as possible.

Despite the fact this section addresses the self-heating process using a PTC thermistor as heated element, a similar method is used to heat the metal resistor of the MOX sensor at a constant temperature, preventing the surrounding flow velocity from changing the heater

temperature and interfere in the odor detection. In this case, although R_3 is still a digital rheostat, its resistance value is user defined, allowing for the detection of multiple odors and increasing the selectivity of the sensor as explained in section 3.2.1.

4.2.2 Temperature Measurement

As referred in the previous section, the temperature compensation of the developed sensor depends on the environment temperature measurement. Thus, an incorrect temperature measurement would compromise the sensor functioning and its reliability. With that said, a stable and effective method must be used for measuring the environment temperature. The high sensitivity of a NTC thermistor makes it an ideal candidate for low cost temperature measurement applications considering a temperature range of $-40°C$ to $125°C$. The existence of NTC thermistors with a SMD termination style, is also an advantage of this type of thermistor, allowing for small size and compact solutions.

Since the analog inputs of micro-controllers can only measure voltage signals, the resistance of the thermistor cannot be measured directly and a further transformation is required. Hence, through a basic voltage divider, it becomes possible to transform the resistance of the thermistor into a measurable voltage signal. The thermistor-based temperature measurement circuit is then made using an additional fixed value resistor and an ADC available in the micro-controller, as shown in Figure 4.10. To minimize the error introduced by the thermistor's self-heating (caused by Joule's effect), the current passing through the thermistor must be kept as low as possible, which can be accomplished by using a thermistor with a high resistance at $25°C$ and a series resistor, R_1, with a high resistance value.

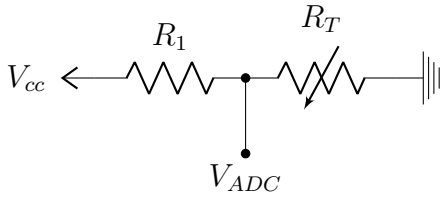

Figure 4.10: Basic voltage divider for temperature measurement.

By analysis of the voltage divider circuit, the resistance of the thermistor, R_T, can be calculated as a function of both the fixed value resistor, R_1, and the ADC voltage, V_{ADC}.

$$V_{ADC} = V_{cc} \cdot \frac{R_T}{R_1 + R_T} \Leftrightarrow R_T = \frac{V_{ADC}}{V_{cc} - V_{ADC}} \cdot R_1 \tag{4.6}$$

In a micro-controller perspective, the voltage signal is seen in a digital manner, so the

method described in Equation (4.6) will not be enough to obtain the resistance of the thermistor. An ADC is a device capable of generating a digital representation of a voltage signal within a specific range where the maximum voltage value corresponds to the maximum ADC value, MAX_{ADC}. This leads to Equation (4.7).

$$R_T = \frac{ADC}{MAX_{ADC} - ADC} \cdot R_1 \tag{4.7}$$

Finally, after the resistance of the thermistor is known and assuming that the Steinhart-Hart coefficients of the NTC thermistor were already calculated as defined in section 3.1.1, the Steinhart-Hart method may be applied to obtain the ambient temperature using a modified form of Equation (3.11).

Note that, although this section refers to the temperature measurement, a similar method is used to measure the resistance of the MOX sensor, allowing the application of concepts defined in section 3.2. Here, a MiCS-5521 sensor was used. It detects reducing gases such as carbon monoxide (CO), hydrocarbons (HC) and volatile organic compounds (VOC) and features a wide detection range and a high sensitivity, a short pre-heating time, miniature dimensions and high resistance to shocks and vibrations, making this sensor the ideal choice.

4.3 Processing

In the previous sections, the transformation of physical quantities, as the airflow velocity, to electrical signals was described - this process is also known as transduction. However, the interpretation of such signals must be later performed using, for instance, a micro-controller. Micro-controllers are small devices, widely used in electronics, containing a processor that can be used as an embedded system, volatile and non-volatile memory and programmable input/output peripherals. The choice of a micro-controller must be made taking into account its application. In this case, the desired functioning of the sensor is shown in Figure 4.11.

Among the various types of micro-controllers there is PIC24FV16KM202 from Microchip, which is suitable for the intended application. It is a 28-pin micro-controller with an operating voltage range from 2.0V up to 5.5V, a 16-bit architecture, a built-in internal oscillator up to 32 MHz PLL clock frequency and 512 bytes of EEPROM data. This micro-controller also makes use of additional useful modules, such as the 12-bit differential ADC, multiple 16-bit timers and the communication interfaces like UART (Universal Asynchronous Receiver Transmitter), SPI (Serial Peripheral Interface) and I^2C (Inter-Integrated Circuit).

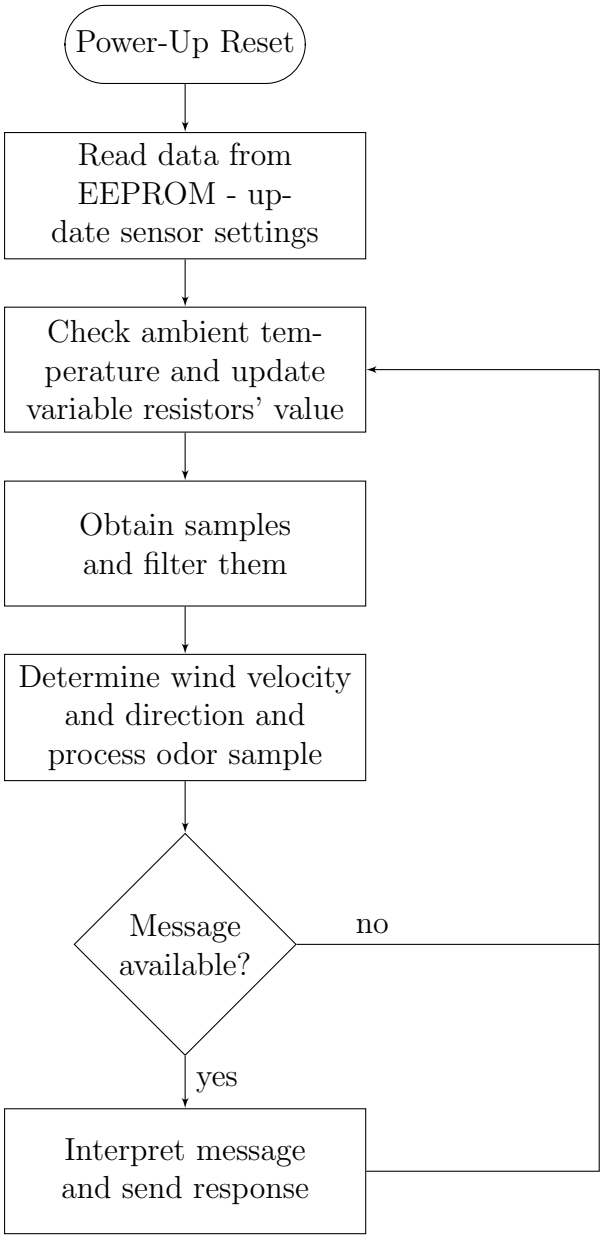

Figure 4.11: Flowchart representing the functioning of the sensor when not in idle mode.

4.3.1 Signal Filtering

The filtering process in a smart sensor is an important step regarding signal conditioning. The first order low-pass RC filter shown in Figure 4.12 is a commonly used solution for removing noise from a signal given its simplicity. However, when the samples are obtained through a digital mean, a configurable infinite impulse response low-pass filter may be achieved via software. From the circuit shown on the right, according to the Kirchhoff's voltage law and the definition of capacitance, the relation between V_{in} and

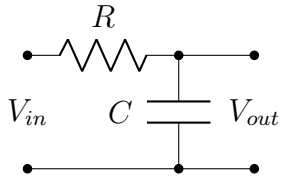

Figure 4.12: Passive low-pass filter.

V_{out} is given by the following equation:

$$V_{in}(t) - V_{out}(t) = Ri(t) = RC \cdot \frac{dV_{out}}{dt} \tag{4.8}$$

By solving the differential equation shown above, one can obtain the time constant of the filter: $\tau = RC$. With that said, the cutoff frequency can also be determined:

$$f_c = \frac{1}{2\pi\tau} = \frac{1}{2\pi RC} \tag{4.9}$$

Finally, the discrete-time implementation of the first order low-pass RC filter can be obtained by discretizing the equation (4.8):

$$\begin{aligned} x[n] - y[n] &= RC \cdot \frac{y[n] - y[n-1]}{\Delta_T} \\ \Leftrightarrow y[n] &= x[n]\left(\frac{\Delta_T}{RC + \Delta_T}\right) + y[n-1]\left(\frac{RC}{RC + \Delta_T}\right) \\ \Leftrightarrow y[n] &= \alpha \cdot x[n] + (1-\alpha) \cdot y[n-1] \quad \text{with} \quad \alpha = \frac{\Delta_T}{RC + \Delta_T} \end{aligned} \tag{4.10}$$

where α is the smoothing factor, y is the filtered output, x is the input, n is the sample index and Δ_T is the sampling period. The cutoff frequency, f_c, can then be calculated as a function of the smoothing factor, α, and the sampling period Δ_T:

$$\tau = RC = \Delta_T\left(\frac{1-\alpha}{\alpha}\right) \rightarrow f_c = \frac{\alpha}{(1-\alpha)2\pi\Delta_T} \tag{4.11}$$

4.3.2 Power Management

The power management is a crucial aspect regarding smart sensors. In this case, the developed sensor must be powered by a 5V/DC voltage source able to provide a current of 200 mA. To save power, the sensor gives the user the possibility to define an idle mode timer. This is an essential feature for environments, such as monitoring networks, where the power consumption must be as low as possible. It allows for the sensor to automatically deactivate some of its modules after a specific time of no usage and automatically activate its modules when their operation is required. While in idle mode, the communication protocol is still completely functional, thus being possible to transit from idle mode to active mode at any time. If a continuous operation is desired, this feature may also be disabled by setting an idle mode timer equal to zero, as specified in the communication protocol.

4.3.3 Communication

This section specifies both the interfaces used for communication and the communication protocol used. Regarding the interfaces used for communication, the choice of such devices should take into consideration how useful they are in a sensor's perspective. Communication using bluetooth, for instance, would not give the sensor any advantages since it is not portable.

In order to allow the use of the sensor in distinct applications, two possibilities of communication were introduced in the sensor: communication through RS-485 or I^2C. The former one, RS-485, is a standard defining data transmission schemes used in serial communications systems which offers robust solutions for transmitting data over long distances ($< 1200\ m$) and in electrically noisy environments with a maximum transmission rate of 10 Mb/s. The fact that multi-point systems are supported in RS-485 makes this standard an excellent solution for sensor networks.

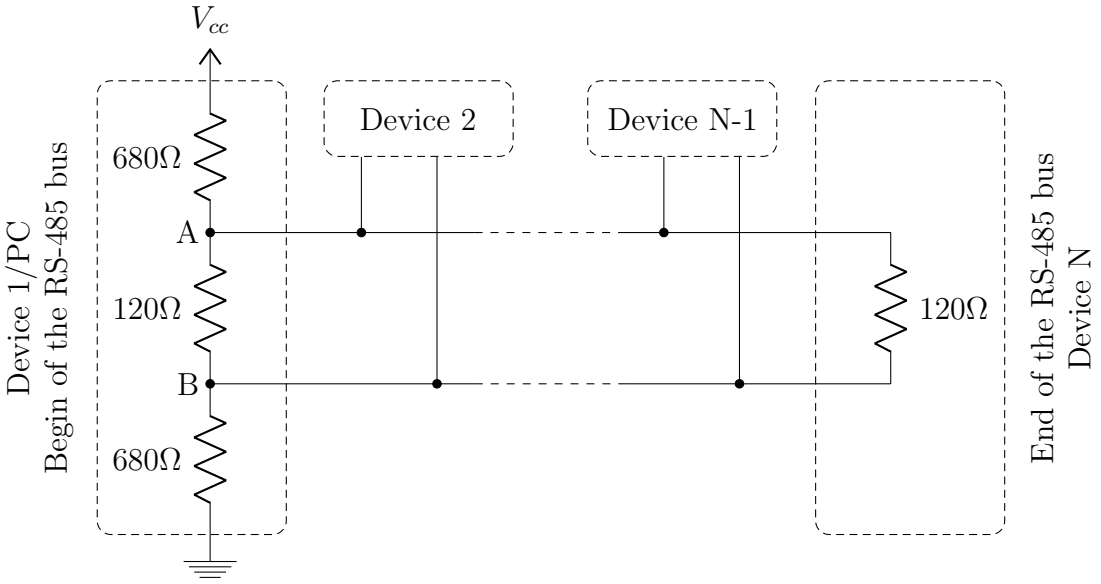

Figure 4.13: RS-485 typical bias network.

As shown in Figure 4.13, the RS-485 standard uses a differential balanced line for communication. To avoid data corruption caused by reflections of fast driver edges, termination resistors with a resistance equal to the characteristic impedance of the line (typically, 120Ω) should be placed, reducing the electrical noise sensitivity. Pull up and pull down resistors may also be placed at the begin of the RS-485 bus to set a known voltage in both lines ensuring that they do not float when not being driven.

For applications, where short distances are required, such as robotics, I^2C can be used

instead of RS-485. This is a synchronous serial computer bus developed by Philips which uses two open-drain bidirectional lines. For this reason, two pull-up resistors are needed when making the physical connection between the devices.

Communicating with the sensor is a crucial task, since all the information may only be obtained through communication. Thus, if for some reason it is not possible to communicate with the sensor or the communication is not being done properly, the sensor itself becomes completely unusable. Therefore, the communication protocol must be robust and functional and ensure the integrity of the received and sent data. Below is represented the typical structure of a message:

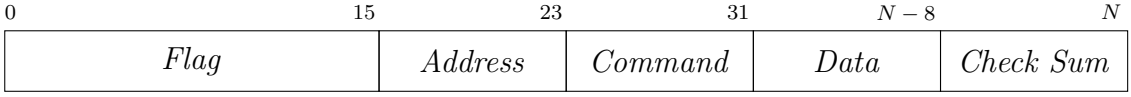

The sensor only accepts messages with a specific header of two bytes (0xA5A5) followed by its address or the broadcasting identifier (0x00), discarding messages sent to other devices. The broadcasting identifier is similar to a global address which can be used when communicating with multiple sensors at the same time. Since all the commands have a fixed size input data, the length of the message is not sent. Finally, after the command and data bytes were sent, a check sum byte must also be sent, giving the sensor the ability to check if the packet was damaged during communication. The check sum byte is calculated as follows:

$$Check\ Sum = \sim(Command_{\ byte} + Data_{\ byte\ 1} + ... + Data_{\ byte\ n})$$

Table 4.1: Commands supported by the sensor

Command	**Default**	**Description**
0x00	0x01	Ping: get the current address
0x01	-	Get the thermistors raw data
0x02		Get the MOX raw data
0x03		Get current ambient temperature
0x04	0x01	Change the sensor's address
0x05	20	Set the temperature difference
0x06	5	Set the sampling time in hundredths of a second
0x07	0	Set the idle time in tenths of a second (0 disables idle mode)
0x08	0	Set MOX heater value
0x09	20	Set the response delay in milliseconds
0x0A	192	Set the baud rate
0x0B	0	Set the temperature check delay in seconds

Table 4.1 shows a list of commands supported by the sensor and their default value. When answering, the structure of the message sent by the sensor is similar to the one previously shown. However, the address and command bytes are discarded and the message header has a different hexadecimal value (0xAAAA). As a consequence, the check sum byte depends on the data bytes only.

Table 4.2: Input and output data for each available command

Command	**Input Data**	**Output Data**
0x00	Null	Current address: [0x01 ... 0xFF]
0x01		[$T1_{HI}$, $T1_{LO}$, $T2_{HI}$, $T2_{LO}$, $T3_{HI}$, $T3_{LO}$, $T4_{HI}$, $T4_{LO}$]
0x02		[MOX_{HI}, MOX_{LO}]
0x03		Ambient temperature (signed): [0x00 ... 0xFF]
0x04	[0x01 ... 0xFF]	
0x05	[0x00 ... 0xFF]	
0x06	[0x00 ... 0xFF]	
0x07	[0x00 ... 0xFF]	
0x08	[0x00 ... 0x8C]	
0x09	[0x0A ... 0xFF]	
0x0A	Baud rate/100: 48, 96 or 192	
0x0B	[D_{HI}, D_{LO}]	

In order to know if a message was successfully received by the sensor and therefore executed, the sensor always sends a response to valid messages - invalid messages will be discarded. Also, the sensor has a default timeout of 100 ms regarding the reception of each byte so, if a message is suddenly interrupted, the sensor will discard the message after the timeout is reached. If the message was successfully sent and parameters were modified, the response data will be equal to the parameters applied. With that said, one is able to know if the parameters were successfully modified by comparing the input data with the response data. Note that the input data for each available command must have a structure as specified in Table 4.2 otherwise the message will be discarded.

5 Tests and Characterization

5.1 Calibration Environment

One of the fundamental steps of this work is to create a calibration environment as reliable and non-intrusive as possible, allowing for an accurate testing of the developed sensor and also permitting to evaluate if the sensor is either working or not-working as expected. The wind tunnel developed in the Institute of Systems and Robotics (ISR), located at the University of Coimbra, is ideal for the testing purposes of this work. It is similar to a $4 \times 3 \times 0.5\ m$ box which can be divided into smaller compartments, containing multiple voltage controlled fans at the outlet so they can pull the air into the tunnel. In order to ensure a laminar fluid flow through the tunnel, *honeycomb* panels were placed at both ends of the wind tunnel, as shown in Figure 5.4, minimizing any disturbances that may compromise the calibration process of the developed sensor.

Keeping in mind that one of the objectives of the current work is to use a calibration environment completely controlled by software so the human interaction is minimal, both the orientation of the sensor and the odor concentration must be controlled by electrical devices somehow connected to a control unit - in this case, a personal computer connected to the communication bus was used as the control unit. On the right, the Dynamixel RX/MX-28 is a robot servo actuator from Robotis equipped with a contact-less magnetic encoder providing the ability to track its speed and shaft position, allowing for 360° turns and a resolution of, approximately, 0.3°. It also offers the possibility of communication either by TTL (transistor–transistor logic) or RS-485, being the ideal choice for the intended environment, allowing to change the orientation of the sensor with a high precision without the need for human intervention.

Figure 5.1: Dynamixel MX-28 from Robotis.

Figure 5.2: Voltage controlled air pump.

The control of the flow velocity and the odor concentration are both performed in a similar way, since the handling of such quantities is realized using devices based on DC motors - electric fans are used for controlling the flow velocity and an air pump, as shown on left, is used to introduce impure air into the wind tunnel. The odor concentration inside the tunnel can therefore be changed by injecting "pure" air into a liquid solution with a specific odor (for instance, alcohol) using an Erlenmeyer flask and an air pump, so the air can circulate within the flask, thus producing impure air. By changing the speed of the air pump, it is possible to inject more or less impure air into the tunnel and also to change the odor concentration level inside the tunnel.

Typically, a DC motor has a high starting torque which is directly proportional to the square of the armature current and, for this reason, a MOSFET or a BJT transistor along with a PWM (Pulse-Width Modulation) control signal may be used as a very good and low cost driver able to provide a quiet and smooth motor operation - Figure 5.3 shows a typical PWM control circuit similar to the one used, where R_1 is a pull-down resistor used to define the default state of the driver. The micro-controller referred in the previous chapter (PIC24FV16KM202) also makes use of a MCCP (Multiple Capture Compare Peripheral) which can be used to generate a PWM signal. Therefore, a PIC-based program was developed to produce the control signal referred above and to communicate with the control unit through RS-485 using a basic communication protocol.

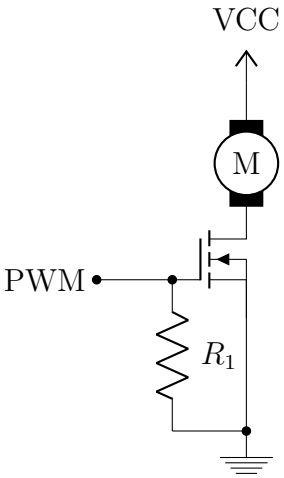

Figure 5.3: Typical PWM control circuit.

All the devices referred above, including the developed sensor, were connected to the same RS-485 communication bus. Thus, through a single Python program it is possible to control all the devices connected to the same communication bus and obtain data from the developed sensor using the communication protocol specified in the previous chapter. Hence, by using the calibration environment shown in the Figure 5.4, one can perform multiple calibration tasks and acquire data automatically.

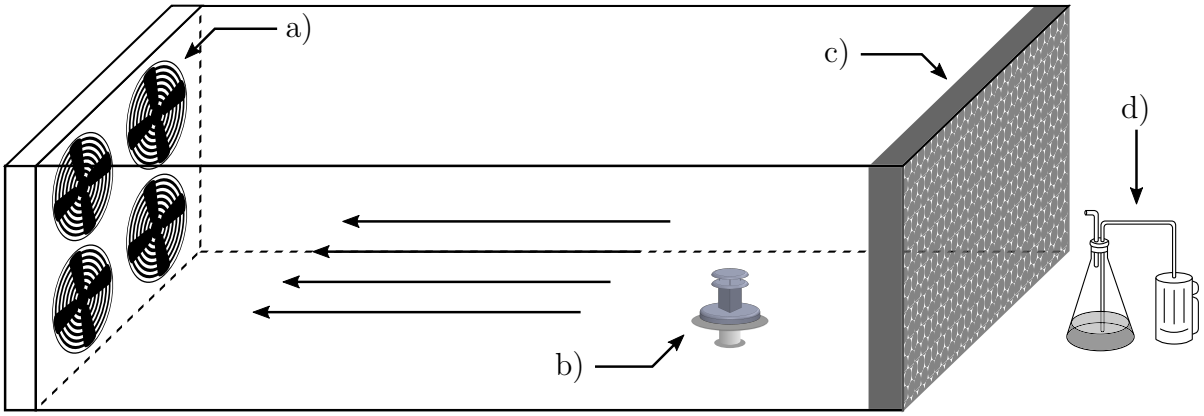

Figure 5.4: Calibration environment for the developed sensor.

Figure 5.4 shows the calibration environment for the developed sensor where a) stands for the voltage controlled fans, b) represents the servo actuator used to change the orientation of the sensor, c) is the inlet *honeycomb* panel (the outlet *honeycomb* panel is located close to the fans) and d) represents the open-loop circuit between the air pump and the Erlenmeyer flask containing a liquid solution used to produce impure air.

5.2 Calibration Results

With the calibration environment described in the previous section, multiple types of tests can be made. In this particular case, the developed sensor will be tested taking into consideration three different situations:

- constant airflow velocity, constant temperature difference and fixed orientation, allowing the analysis of the sensor's response to the presence of an odor;
- constant temperature difference, fixed orientation and variable airflow velocity, so one can analyze the response of the sensor for different airflow velocities;
- constant airflow velocity, fixed temperature difference and variable orientation, allowing to analyze the response of the sensor for multiple angles of incidence.

In this section it is intended to present the results obtained for the three cases previously mentioned, which can be organized as a set of 4 tests: detecting odors; measuring the odor concentration; measuring the airflow velocity and measuring the airflow direction.

5.2.1 Test 1 - Odor Detection

The main objective of the first test is to verify if the developed sensor is able to simply detect an odor and, in affirmative case, analyze its response time and recovery time after the

exposure to impure air. In this case, since the MiCS-5521 odor sensor is commonly used to detect volatile organic compounds as referred in section 4.2.2, ethyl alcohol can be used in tests regarding the odor measuring - ethyl alcohol is an organic compound mainly composed of ethanol which can be found at most of the pharmacies.

With that said, this test will be based on an analysis divided into three simple steps: introduction of pure air at a constant flow rate; injection of impure air, maintaining the flow rate, in order to analyze the response time of the sensor and, finally, injection of pure air, similarly to the first step, so one can analyze the recovery time of the sensor.

Ideally, the sensor should present a unit step response when detecting odors but, in practice, such is not possible, since factors as the fluid flow velocity, environment temperature and humidity must be kept into consideration. In addition, the heating temperature of the MOX sensor's metal resistor is another factor that, although it is not the object of study of this work, is quite important. The Figures 5.5 and 5.6 show the results obtained for a fluid flow velocity of 0.6 m/s and 2.2 m/s, respectively, and a 10 seconds time delay between steps - the red dashed lines mark the transition between the steps mentioned above.

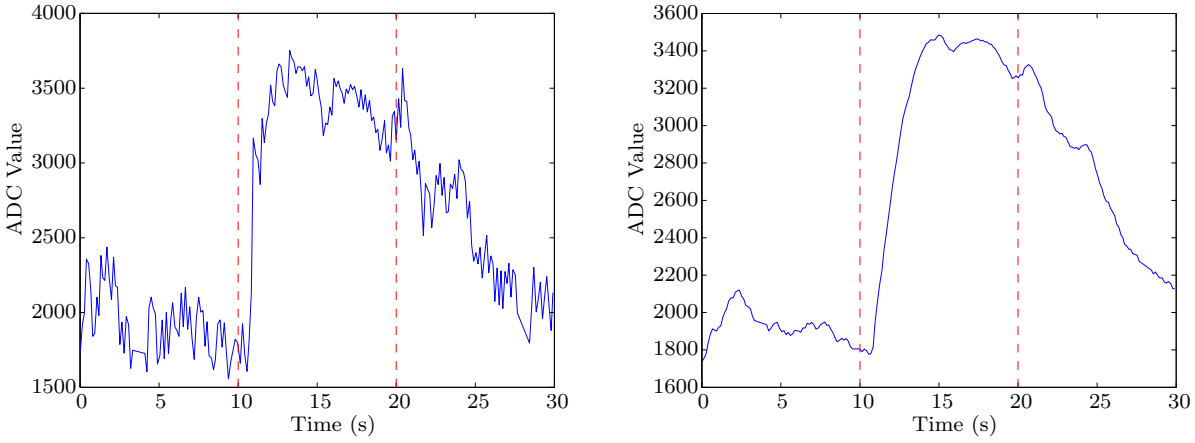

(a) Raw data.

(b) Filtered data.

Figure 5.5: Test 1 results obtained considering a fluid flow velocity of 0.6 m/s.

The results presented above show that, for a velocity of 0.6 m/s, the sensor takes about 1 second to detect the presence of an odor, which can be explained by the distance between the sensor and the inlet of the wind tunnel. The sensor has proved to have a very good response to low fluid flow velocities. However, the lower the velocity is, the higher is the recovery time of the sensor. Along with this test, multiple tests were made considering fluid flow velocities between 0.6 and 2.2 m/s to analyze the influence of the flow velocity in the odor detection.

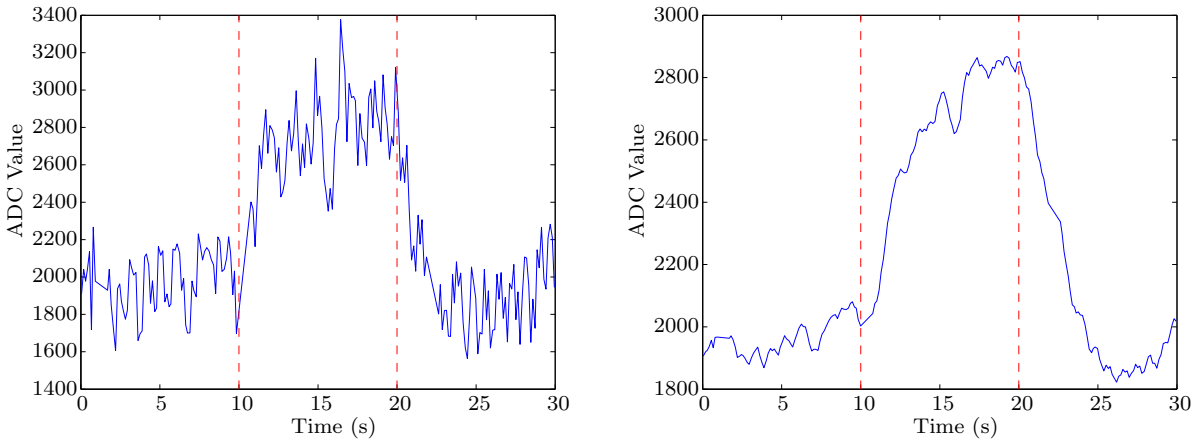

(a) Raw data.

(b) Filtered data.

Figure 5.6: Test 1 results obtained considering a fluid flow velocity of 2.2 m/s.

When submitted to a flow velocity of 2.2 m/s, as shown in Figure 5.6, the sensor detected the presence of an odor almost instantly and its recovery time was much lower than when submitted to a flow velocity of 0.6 m/s, confirming what was previously said. On the other hand, the sensor presented a noisier response than in the first case, thus requiring filtering. By applying a low-pass filter similar to the one referred in section 4.3.1 with a 85% smoothing factor, most of the noise was removed and the sensor presented a smooth response regardless of the flow velocity.

As a conclusion, the results of this test were as expected, demonstrating that the developed structure does not affect the detection of odors.

5.2.2 Test 2 - Odor Concentration

The purpose of the second test is to verify if the sensor is able to measure the odor concentration and analyze the response of the sensor to sudden variations of the odor concentration. In consideration of the foregoing, the second test will be similar to the previous one but, in this case, there will exist multiple steps where each one corresponds to a different value of odor concentration, instead of a single step where the odor concentration is maximum. Therefore, this test can be divided into three different parts, where the flow velocity is kept at a constant value: injection of pure air; gradual increase of the odor concentration within the wind tunnel step by step and, ultimately, new injection of pure air.

The air pump used in this test does not have enough precision to allow a precise mass flow control, resulting in unknown concentration values along the testing process. A precise test would require a closed-loop system where the flow velocity and the odor concentration

were controlled by the same device. Such would require expensive materials and a much more complex calibration environment. As a workaround for this problem, the duty cycle of the PWM signal used to control the air pump responsible for the injection of impure air into the wind tunnel will be used as a reference value for the odor concentration within the wind tunnel.

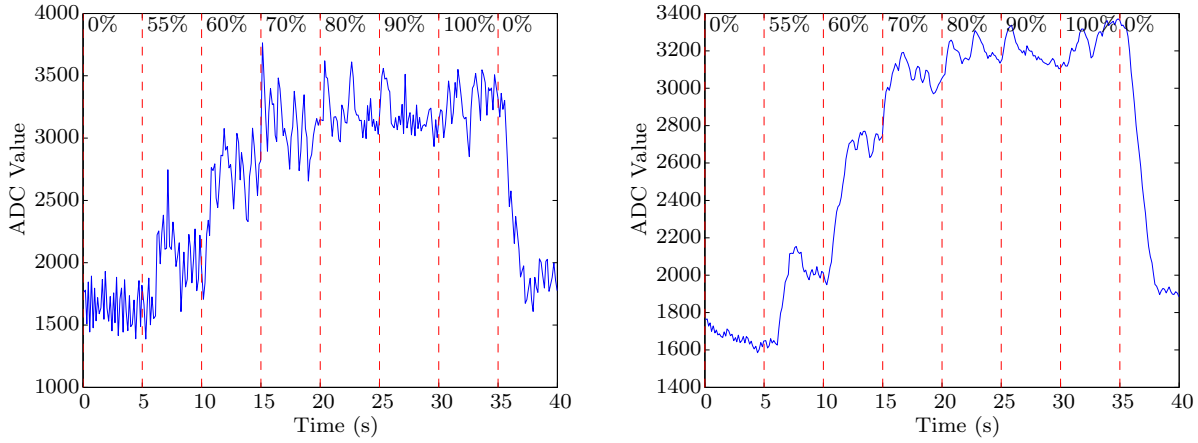

(a) Raw data.

(b) Filtered data.

Figure 5.7: Test 2 results obtained considering a fluid flow velocity of 1.2 m/s.

Figure 5.7 shows the results obtained from testing the sensor with a flow velocity of 1.2 m/s. Overall, the results were quite satisfactory, proving that using a MOX sensor for measuring the odor concentration is a viable option, featuring a high sensitivity and a considerable detection range.

When developing the odor compass, the measurement circuit of the MOX sensor was designed in such a manner that it would not interfere with the functioning nor damage the MOX sensor, resulting in the choice of a resistor with a medium/high resistance value as the resistor in series with the MOX sensor. This resulted in a small measuring range regarding the odor detection, as shown in the Figure above - when no odor is being detected, the ADC measures a value of 1500, approximately. To improve the measuring range of the MOX sensor, a resistor with a lower resistance value may be used, thus increasing the sensitivity of the MOX sensor and guaranteeing a wider measuring range.

Figure 5.8 shows that the Equation (3.13) can be used to relate the odor concentration with the resistance of the MOX sensor. To note that, in this case, the ADC Values shown in the Figure are inversely proportional to the resistance of the MOX sensor due to the used measurement circuit.

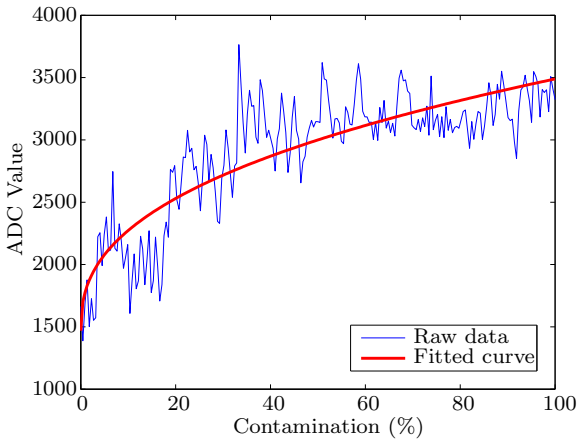

Figure 5.8: Interpolation of data set from Test 2's procedure.

5.2.3 Test 3 - Measuring the Airflow Velocity

The third test consists in maintaining a constant temperature difference between the heated element and the ambient temperature, a fixed orientation and variable flow velocity, so one can study the response of the developed sensor to different airflow velocities taking into consideration only one dimension. Thus, similarly to the previous test, this test will be divided into multiple steps, where each step corresponds to a different flow velocity which results from a gradual increase of the fans speed using the control circuit shown in Figure 5.3.

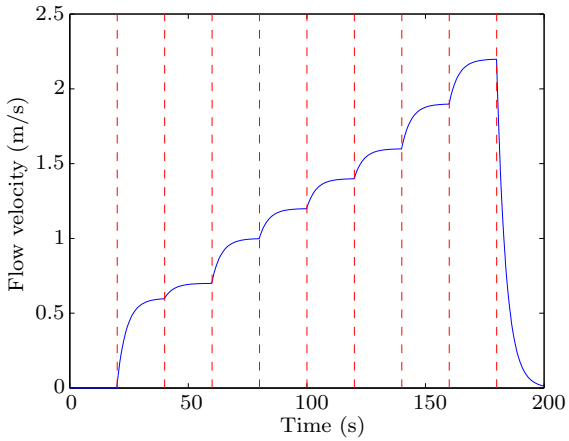

Figure 5.9: Flow velocity inside the wind tunnel.

The fans used in this test procedure are devices which have a high inertia due to their large size and weight. This results in a slow response to variations of the PWM control signal, being necessary some time so the fans can reach the desired speed. Besides, since the fans do not have a brake system, only friction will act when a speed reduction is desired, giving rise to measurement errors. By using a commercial hot-wire anemometer, it was possible

to verify that, along a complete test, the airflow velocity inside the wind tunnel could be approximately described by the curve shown in Figure 5.9.

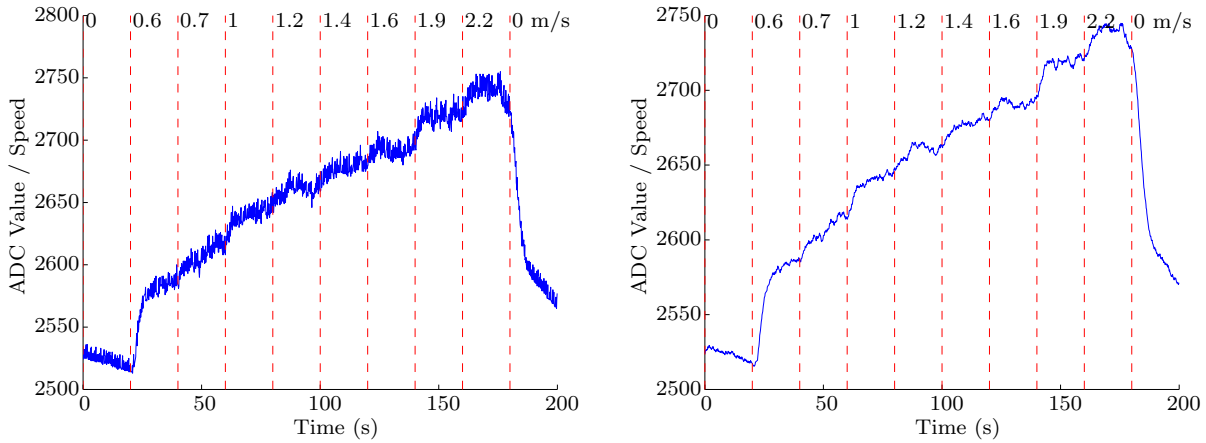

(a) Raw data.

(b) Filtered data.

Figure 5.10: Test 3 results obtained considering a temperature difference of 40°.

The results obtained from measurement were quite satisfactory. As expected, the high inertia of the fans was noticeable on the measured data, being the latter similar to the expected flow velocity inside the wind tunnel. Once again, the filtering process has proved to be fundamental regarding the data analysis, removing part of the noise of the measured data.

Along with this test, multiple tests considering different temperature differences were made and the filtered data obtained from each test was identical to the data shown in Figure 5.10. However, it was noted that the higher the temperature difference, the higher the sensitivity and the noise of the response, being this an expected result taking into consideration the Equation (3.7).

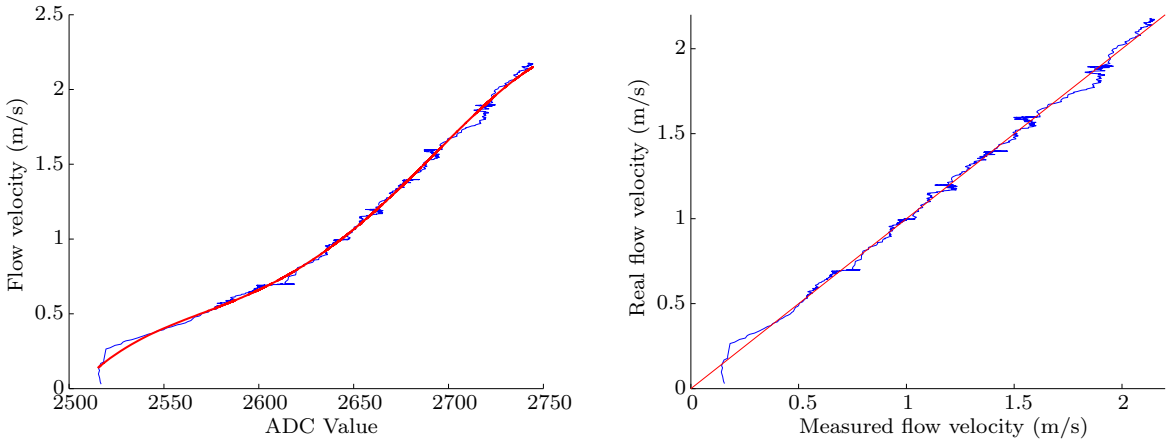

(a) 4th degree interpolation.

(b) Data comparison.

Figure 5.11: Interpolation of data set from Test 3's procedure.

Using the *polyfit()* function from MATLAB, the fourth-order polynomial function which best relates the measured ADC data with the flow velocity inside the wind tunnel was calculated, being the result shown in Figure 5.11a. This graph was obtained by using the *polyval()* function with the previously calculated coefficients and the measured ADC data. Despite there is a considerable error introduced by the fans responsible for producing the airflow, the fourth-order polynomial function calculated exhibited a very small maximum absolute error (less than 0.1 m/s) and a mean absolute error of 0.0245 m/s for the tested range of velocities, proving that thermal methods for measuring the flow velocity can be very precise and accurate. To note that a comparison between the measured flow velocity and the flow velocity inside the wind tunnel was made (Figure 5.11b), so one could better analyze the deviation of the sensor's measured velocity.

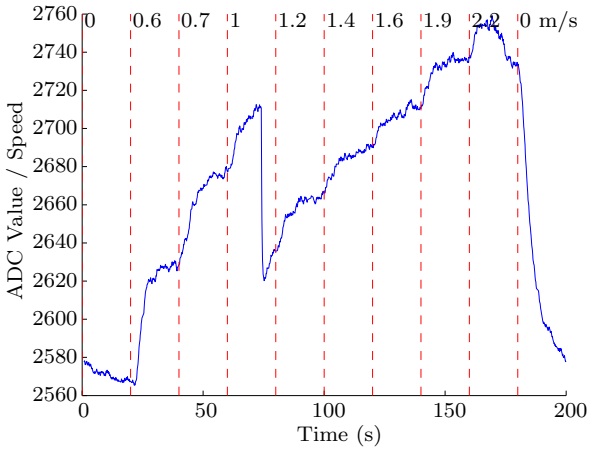

Figure 5.12: Response of the sensor when compensating the temperature.

When realizing the tests related to the measurement of the airflow velocity, it was possible to verify the effect of the temperature compensation on the response of the sensor. Figure 5.12 shows a specific case where the temperature compensation occurred when realizing a test procedure. In this case, the temperature difference between the heated element and the environment temperature was, initially, higher than desired. Approximately at the 77 seconds mark, when the sensor compensated the temperature, the gain of the sensor's response decreased abruptly. This abrupt decrease can be explained by the high resistance of each step of the digital rheostat used to compensate the temperature. The way to improve the developed sensor in such a manner that the temperature compensation does not produce significant variations in the sensor's response will be further discussed in the Future Work section, 6.1.

5.2.4 Test 4 - Measuring the Airflow Direction

The fourth and last test consists in maintaining both the airflow velocity and the temperature difference between the heated elements and the environment temperature at a constant value and vary the sensor's orientation. Although in a real life situation the airflow velocity will certainly vary through time, it will be kept constant in order to facilitate the results' analysis - any voltage variations of the heated elements may only result from changes regarding the sensor's orientation. Thus, using the servo actuator referred in section 5.1, one can modify the sensor's orientation in order to simulate the incidence of an airflow considering multiple directions. Finally, the response of the sensor may be analyzed by performing a complete turn of the developed sensor and, at the same time, measuring the voltage of all heated elements.

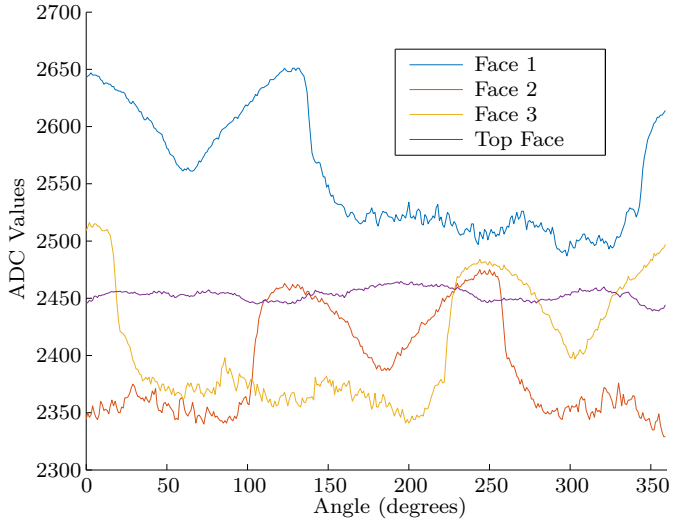

Figure 5.13: Test 4 results obtained considering a temperature difference of 30° and a flow velocity of 1.8 m/s.

Figure 5.13 shows the results obtained when performing the test described above. Since the top face thermistor of the developed sensor is responsible for measuring the flow velocity and taking into consideration that the flow velocity was kept constant throughout this test, a non-variable response was expected. In fact, the response of the top face thermistor shown in the Figure above is approximately constant, however it contains small oscillations which can be explained by the existence of small turbulence effects inside the wind tunnel. The remaining thermistors (faces 1, 2 and 3) are, therefore, the ones responsible for measuring the airflow direction. Similarly to the referred in section 4.1, in a complete turn of the sensor, the responses regarding the thermistors located in the center of each face of the triangular

structure present a 120° offset from each other, proving that it is possible to measure the airflow direction by relating all the responses considering the existence of three measurement regions.

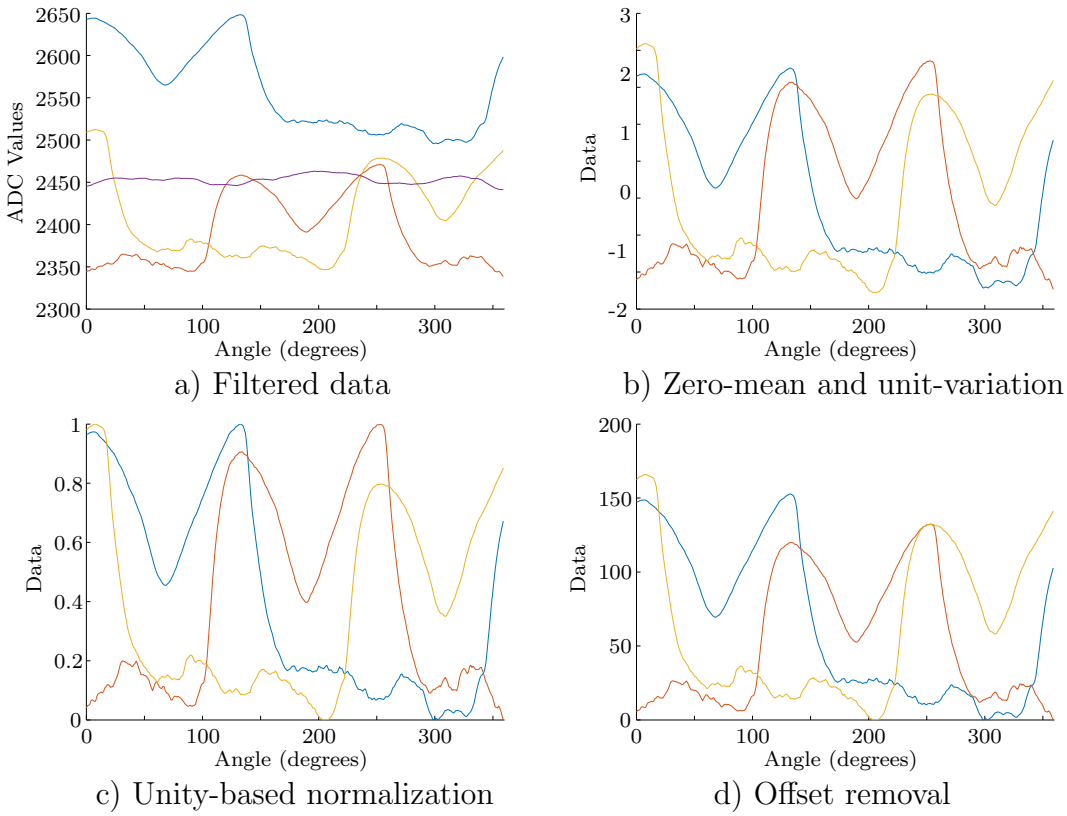

Figure 5.14: Analysis of the results obtained from Test 4.

Ideally, the three response curves should contain the same range of values. However, such was not possible due to small differences between the heated elements used, leading to a necessary data pre-processing so the response can be analyzed. Both the feature rescaling and the feature standardization are methods widely used in machine learning algorithms where the measured data must be normalized. The first method consists in a unity-based normalization which can be generalized to restrict the range of values in the dataset between two known limits, a and b, as shown by Equation (5.1), while the second method consists in a normalization where the values of each dataset have a zero-mean, $\bar{f}$, and unit-variance, σ, as shown by Equation (5.2).

$$f'(x) = a + \frac{f(x) - \min(f)}{\max(f) - \min(f)} \cdot (b - a) \tag{5.1}$$

$$f'(x) = \frac{f(x) - \bar{f}}{\sigma} \tag{5.2}$$

Although both methods require a calibration routine in a sensor's side, the unity-based normalization is the most simple yet effective to apply, being only necessary to obtain both the maximum and minimum values of each sensing point when performing the calibration routine. For this reason, the unity-based normalization was the method used regarding the data pre-processing.

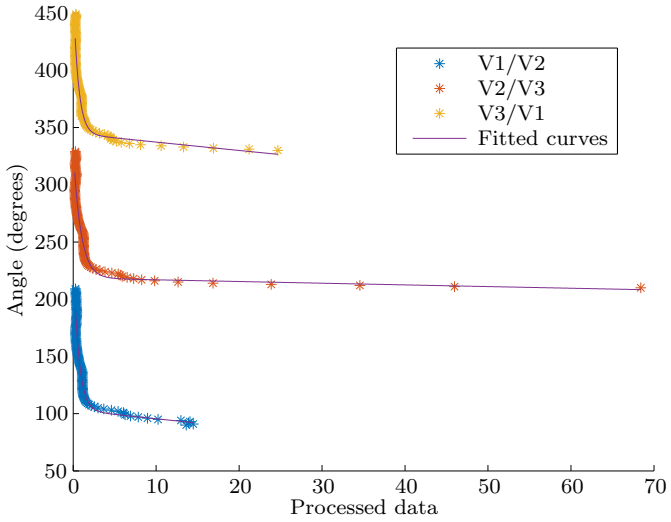

Figure 5.15: Curve fitting using a two-term exponential model.

As previously mentioned, the response of the sensor can be divided into three measurement regions, where each one characterizes a specific angular region considering a range of 120°, as shown in Figures 5.14c and 5.15. Therefore, one can determine the region in which a measurement is located by analyzing all the thermistors contribution using the Algorithm 1: the lowest contributor is discarded and the ratio between the two highest contributors is used to obtain the airflow direction.

Algorithm 1 Algorithm used to measure the airflow direction

procedure CALCULATEAIRFLOWDIRECTION
    $t_1, t_2, t_3 \leftarrow GetFilteredData()$ ▷ Get the filtered data
    $t_1, t_2, t_3 \leftarrow NormalizeData(t_1, t_2, t_3)$ ▷ Normalize the obtained data
    if $t_3 < t_1$ **and** $t_3 < t_2$ **then** ▷ t_3 is the lowest contributor
        $angle \leftarrow f_1(t_1/t_2)$ ▷ f_1 relates the current angle with t_1/t_2
    else if $t_1 < t_2$ **and** $t_1 < t_3$ **then** ▷ t_1 is the lowest contributor
        $angle \leftarrow f_2(t_2/t_3)$ ▷ f_2 relates the current angle with t_2/t_3
    else ▷ t_2 is the lowest contributor
        $angle \leftarrow f_3(t_3/t_1)$ ▷ f_3 relates the current angle with t_3/t_1
    end if
    $angle \leftarrow WrapTo360(angle)$ ▷ assure that $angle$ is between 0 and 360
    return $angle$
end procedure

Overall, the developed sensor along with the developed algorithm for measuring the airflow direction presented satisfactory results, having a 3% mean absolute error and a 10% maximum absolute error. It was noted that the absolute error tends to increase as the airflow becomes perpendicularly incident with one of the sensor's faces due to the low contribution of the remaining two thermistors. However, the sensor's response could be enhanced by rounding the corners of the triangular structure responsible for the airflow direction measurement, thus promoting the reattachment of the flow on the lateral faces and increasing the contribution of the sensing elements located in the triangular structure. Other option to improve the sensor's response consists in dividing it into six measurement regions, where each one characterizes a range of 60°, instead of 3 regions regarding a range of 120° each one. As a conclusion and in addition to the previously discussed, the sensor demonstrated to be accurate and precise enough both for use in robotics and for use in sensor networks, fulfilling the objectives of this work.

6 Conclusion

In this thesis, multiple anemometers as well as gas sensors were described. Their advantages and disadvantages were then analyzed in order to develop an odor compass. Since electrochemical gas sensors along with thermal anemometry have shown to be advantageous regarding the development of an odor compass, the developed sensor was based on thermal methods for measuring the flow properties and a metal oxide gas sensor to measure the odor's concentration.

Figure 6.1: Photograph of the final product.

The temperature compensation method for heating the sensing elements was one of the challenges of this work. The solution found consisted of using digital rheostats to calibrate the reference branch of the Wheatstone bridge, making it possible to have software controllable self-heating elements. This temperature compensation method allows to change the temperature difference between the heated element and the environment, thus being very useful for decreasing the power consumption of the sensor or increasing its sensitivity.

Overall, the developed sensor presented satisfactory results, as initially expected, and the proposed objectives were accomplished. The solution described in chapters 4 and 5 demonstrated to be effective, having an estimated cost of 70 euros and with a calibration process practically fully automated. Although the results obtained are quite satisfactory, it is important to keep in mind that solutions for the odor source localization may also consider smaller thermal anemometers, such as thermal anemometers based on MEMS hot-film sensors.

6.1 Future Work

Despite the developed sensor works as expected, there are several improvements that can be done as future work.

The sensor was initially designed to support a 5V voltage. However, this voltage limits the sensor's sensitivity, by restricting the heating temperature. This restriction could be removed by using a DC-DC step-up converter, increasing the voltage from 5V to 12V. To note that this change would require the insulation of the circuits responsible for the self-heating of the sensing elements and also some additional signal conditioning in order for the micro-controller's ADCs to be able to measure voltages superior than their internal reference.

Finally, as previously shown in Figure 5.12, the actual temperature compensation method may cause an abrupt change in terms of sensor's response. This compensation could be smoother either by using digital rheostats with a higher resolution or redesigning the branch of the Wheatstone bridge responsible for temperature compensation so that each step of the digital rheostat has a smaller influence on the heated element's temperature.

Bibliography

[1] M. Brattoli, G. De Gennaro, V. De Pinto, A. Demarinis Loiotile, S. Lovascio, and M. Penza, "Odour detection methods: Olfactometry and chemical sensors," *Sensors*, vol. 11, no. 5, pp. 5290–5322, 2011.

[2] R. Probst, G. Grevers, and H. Iro, *Basic Otorhinolaryngology: A Step-by-step Learning Guide*, ser. Thieme Publishers Series. Thieme, 2005. [Online]. Available: https://books.google.pt/books?id=X0oXV0xrU5sC

[3] P. M. Wise, M. J. Olsson, and W. S. Cain, "Quantification of odor quality," *Chemical senses*, vol. 25, no. 4, pp. 429–443, 2000.

[4] K. Persaud and G. Dodd, "Analysis of discrimination mechanisms in the mammalian olfactory system using a model nose." *Nature*, vol. 299, no. 5881, pp. 352–355, 1982.

[5] D. James, S. M. Scott, Z. Ali, and W. T. O'hare, "Chemical sensors for electronic nose systems," *Microchimica Acta*, vol. 149, no. 1-2, pp. 1–17, 2005.

[6] C. Di Natale, D. Salimbeni, R. Paolesse, A. Macagnano, and A. D'Amico, "Porphyrins-based opto-electronic nose for volatile compounds detection," *Sensors and Actuators B: Chemical*, vol. 65, no. 1, pp. 220–226, 2000.

[7] N. A. Rakow and K. S. Suslick, "A colorimetric sensor array for odour visualization," *Nature*, vol. 406, no. 6797, pp. 710–713, 2000.

[8] O. S. Wolfbeis, "Fluorescence optical sensors in analytical chemistry," *TrAC Trends in Analytical Chemistry*, vol. 4, no. 7, pp. 184–188, 1985.

[9] S. Fanget, S. Hentz, P. Puget, J. Arcamone, M. Matheron, E. Colinet, P. Andreucci, L. Duraffourg, E. Myers, and M. Roukes, "Gas sensors based on gravimetric detection—a review," *Sensors and Actuators B: Chemical*, vol. 160, no. 1, pp. 804–821, 2011.

[10] O. Rudko, "Design of a low-frequency sound sensor inspired by insect sensory hairs," Master's thesis, M. Sc. thesis, State University of New York at Binghamton, Department of Mechanical Engineering, 2001.

[11] T. C. Karalar, "An acoustic digital anemometer," Master's thesis, Citeseer, 2002.

[12] F. Durst, A. Melling, and J. H. Whitelaw, "Principles and practice of laser-doppler anemometry," *NASA STI/Recon Technical Report A*, vol. 76, p. 47019, 1976.

[13] Sensirion, *Sensirion Mass Flow Meters SFM4100 Datasheet*, 2013, rev. 1.3.

[14] H. I. Inc., *Airflow Sensors Line Guide*, 2014.

[15] H. Bruun, *Hot-wire Anemometry: Principles and Signal Analysis*, ser. Oxford science publications. Oxford University Press, 1995. [Online]. Available: https://books.google.pt/books?id=PkAnIqXGkY0C

[16] J. Weiss and G. Comte-Bellot, "Electronic noise in a constant voltage anemometer," *Review of scientific instruments*, vol. 75, no. 5, pp. 1290–1296, 2004.

[17] L. Osório, "Localização tridimensional de fontes de odor em robótica móvel," Master's thesis, Universidade de Coimbra, 2011.

[18] A. S. Cubukcu, E. Zernickel, U. Buerklin, and G. A. Urban, "A 2d thermal flow sensor with sub-mw power consumption," *Sensors and Actuators A: Physical*, vol. 163, no. 2, pp. 449–456, 2010.

[19] H.-B. Liu, N. Lin, S.-S. Pan, J. Miao, and L. K. Norford, "High sensitivity, miniature, full 2-d anemometer based on mems hot-film sensors," *IEEE Sensors Journal*, vol. 13, no. 5, pp. 1914–1920, 2013.

[20] Y.-T. Wei, Q.-H. Meng, Y.-Q. Jing, Y.-J. Liu, and M. Zeng, "A portable odor-tracing instrument," *IEEE Transactions on Instrumentation and Measurement*, vol. 65, no. 3, pp. 631–642, 2016.

[21] H. Ishida, A. Kobayashi, T. Nakamoto, and T. Moriizumi, "Three-dimensional odor compass," *IEEE Transactions on Robotics and Automation*, vol. 15, no. 2, pp. 251–257, 1999.

[22] L. Marques, N. Almeida, and A. De Almeida, "Olfactory sensory system for odour-plume tracking and localization," in *Sensors, 2003. Proceedings of IEEE*, vol. 1. IEEE, 2003, pp. 418–423.

[23] J. P. Bentley, *Principles of measurement systems*. Pearson Education India, 1995.

[24] L. J. F. Marques, "Navegação de robôs móveis usando olfacto," Ph.D. dissertation, Universidade de Coimbra, 2004.

[25] F. Hossein-Babaei and A. Amini, "A breakthrough in gas diagnosis with a temperature-modulated generic metal oxide gas sensor," *Sensors and Actuators B: Chemical*, vol. 166, pp. 419–425, 2012.

[26] N. Almeida, L. Marques, and A. T. de Almeida, "Multi-point systems for remote monitoring of air quality," in *Sensors for Environmental Control: Proceedings of the International Workshop on New Developments on Sensors for Environmental Control (ENVSENS), S. Cesarea Terme, Lecce, Italy, 27-29 May 2002*. World Scientific Pub Co Inc, 2003, p. 168.

[27] C. Walter Frei, "Introduction to turbulence modeling," http://www.comsol.com/blogs/which-turbulence-model-should-choose-cfd-application/.

[28] F. P. Incropera and D. P. De Witt, *Fundamentals of heat and mass transfer*. John Wiley and Sons, 1985.

[29] L. Carassale, A. Freda, and M. Marrè-Brunenghi, "Experimental investigation on the aerodynamic behavior of square cylinders with rounded corners," *Journal of Fluids and Structures*, vol. 44, pp. 195–204, 2014.

[30] I. Zhdan, V. Stulov, P. Stulov, and L. Turchak, "Drag coefficients for bodies of meteorite-like shapes," *Solar System Research*, vol. 41, no. 6, pp. 505–508, 2007.

[31] N. K, "Influence of corner geometry on the flow structure and flow characteristics for flow past a square cylinder at re=150," *International Journal of Research in Aeronautical and Mechanical Engineering*, vol. 2, no. 12, pp. 32–41, 2014.

Appendix A

Sensor Design and Dimensions

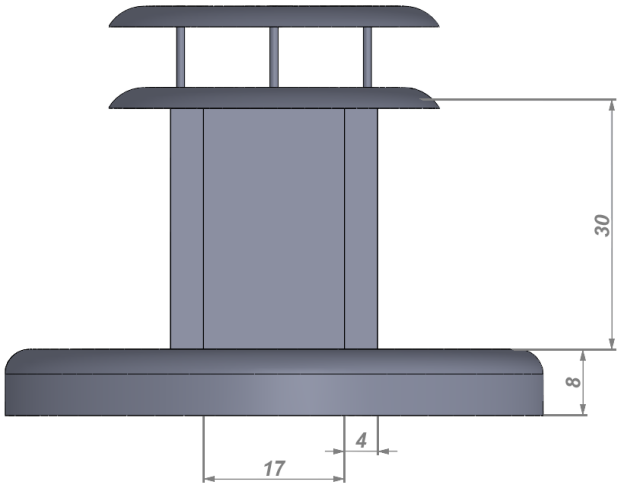

(a) Front view.

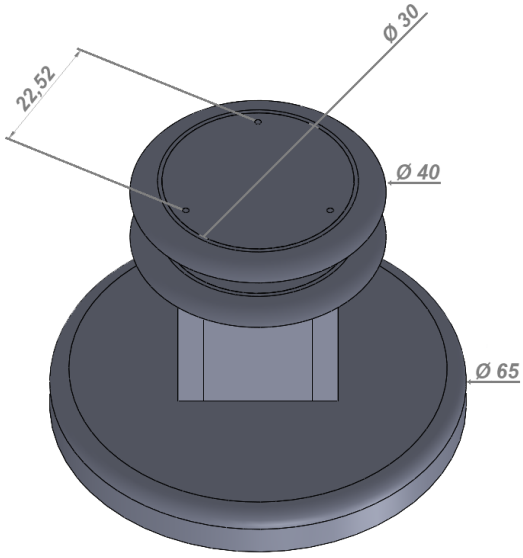

(b) Top view.

Appendix B

Printed Circuit Board Design and Circuit Schematics

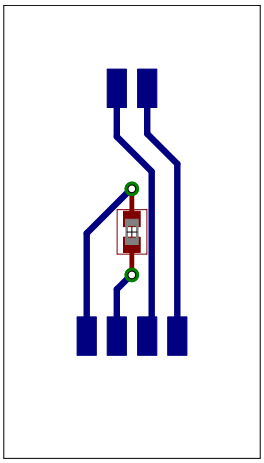

(a) 4-pin lateral face.

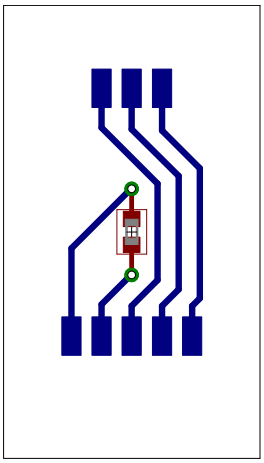

(b) 5-pin lateral face.

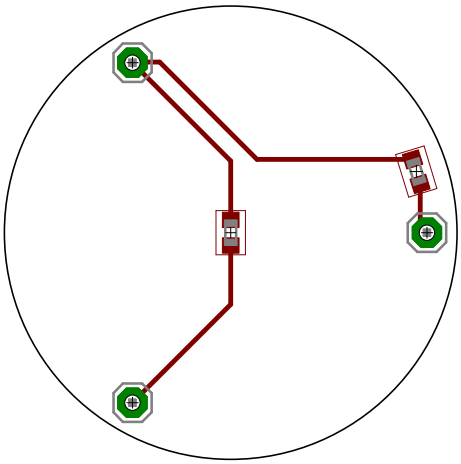

(c) Top plate.

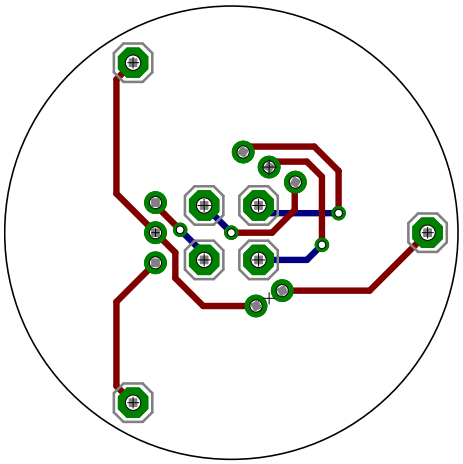

(d) Bottom plate.

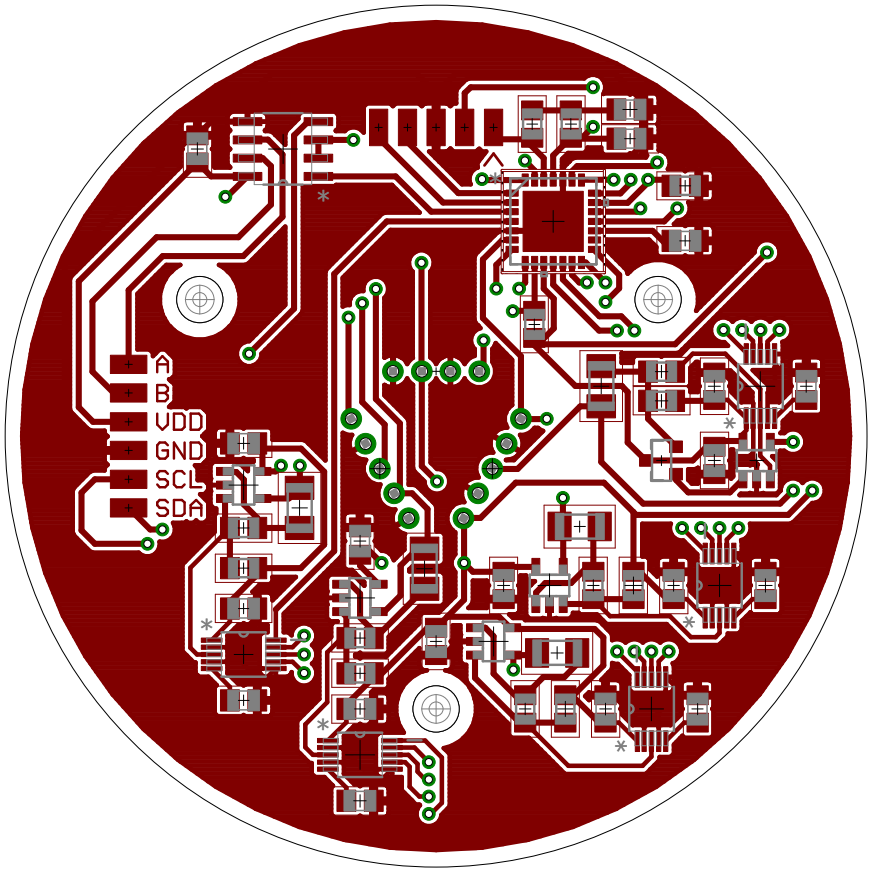

(a) Processing unit - top view.

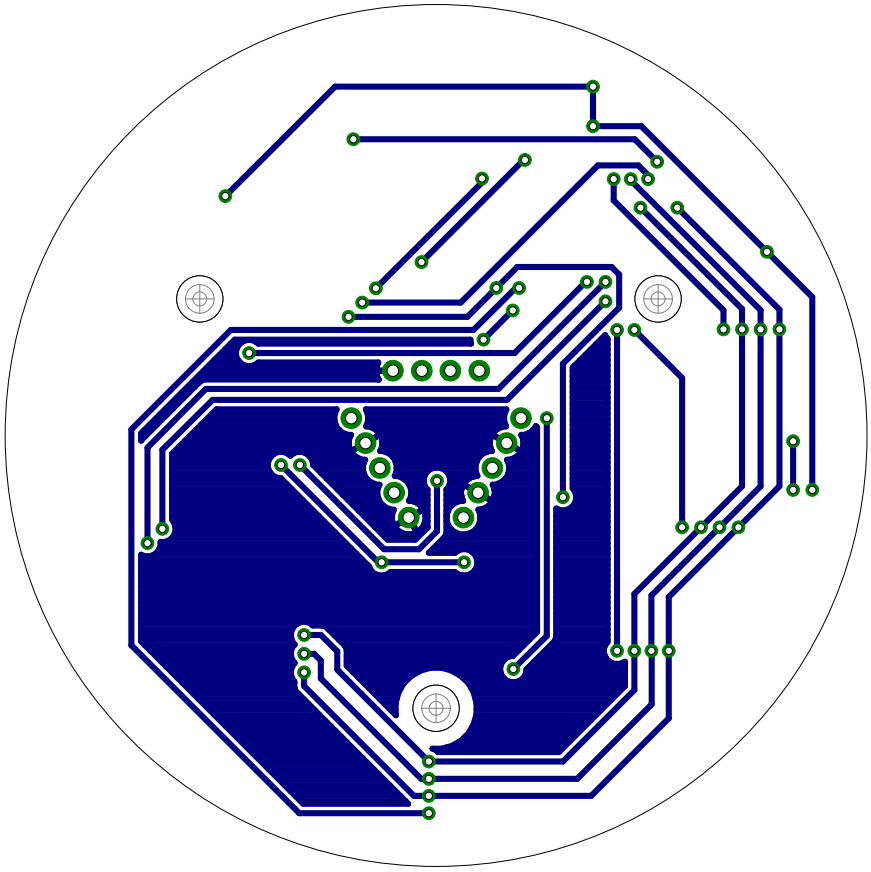

(b) Processing unit - bottom view.

Pinout

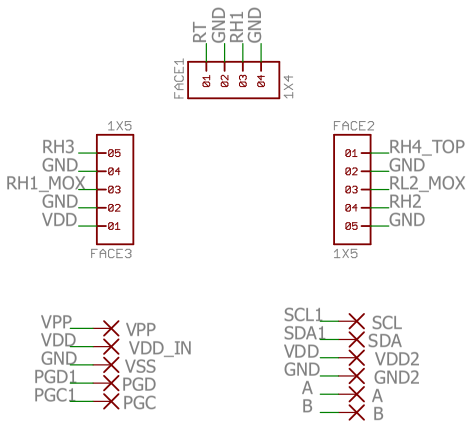

Micro-controller

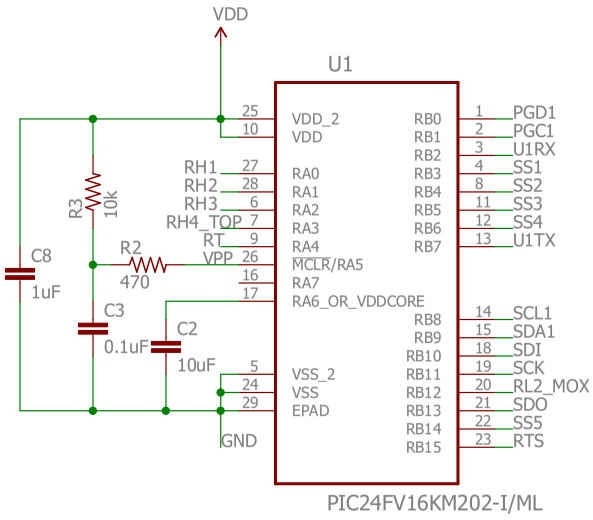

Communication

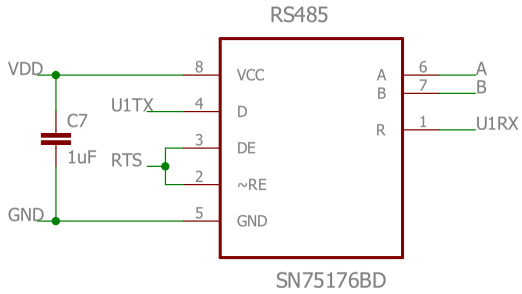

MOX heating

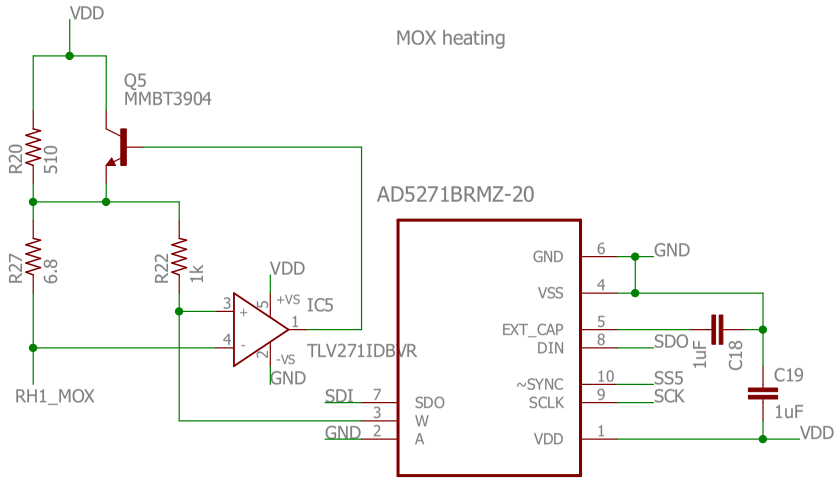

Decoupling capacitor OpAmp

Temperature Sensor

MOX sensor

Odor Compass	2016/2017
Institute of Systems and Robotics	
José Caetano	Sheet: 1/2

Self-Heating and temperature compensation

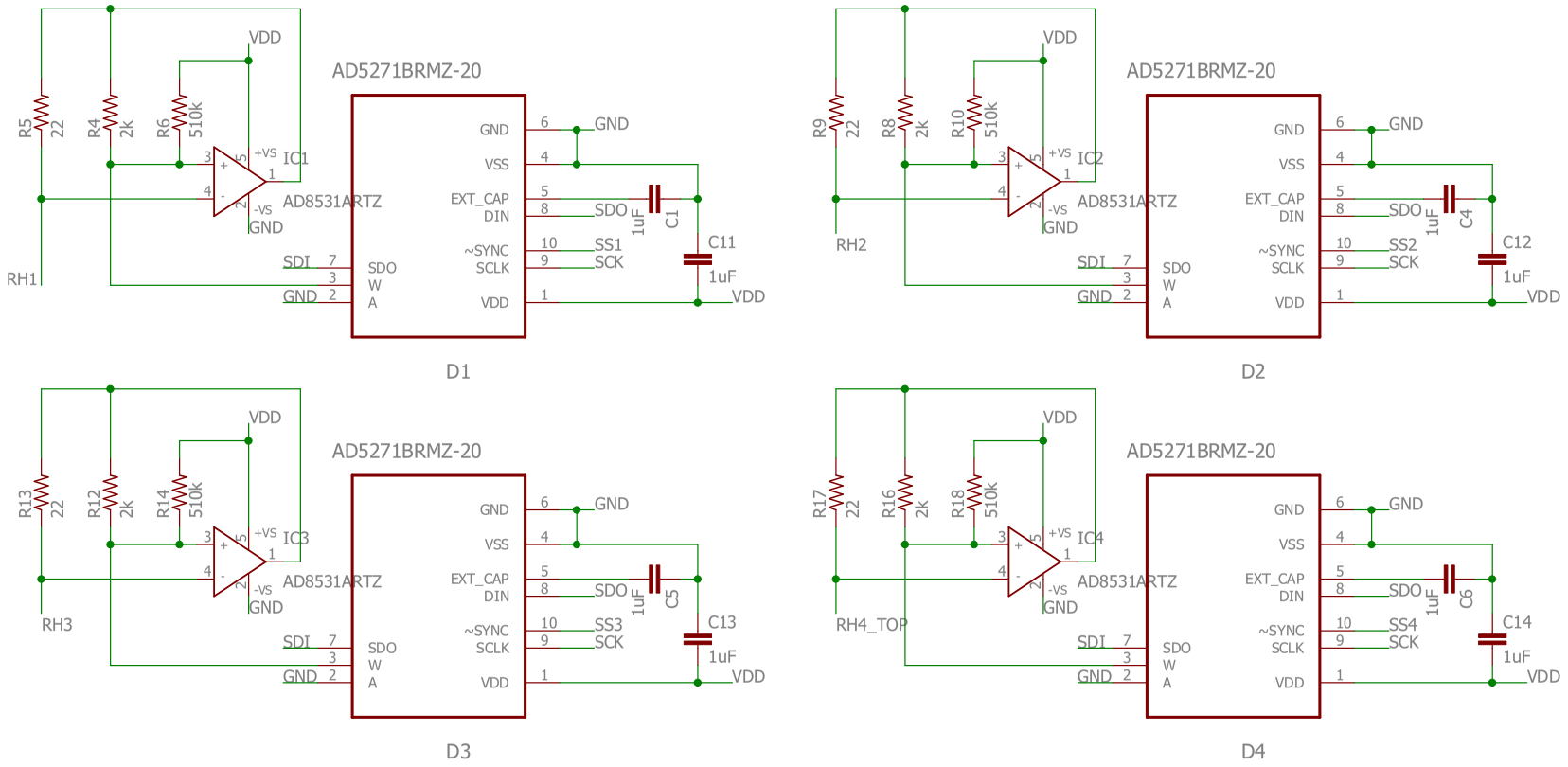

Decoupling capacitors - OpAmps

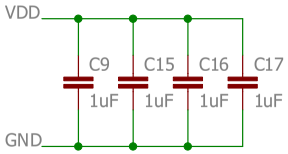

Odor Compass	2016/2017
Institute of Systems and Robotics	
José Caetano	Sheet: 2/2